Biochimica et Biophysica Acta 1832 (2013) 249–262

Contents lists available at SciVerse ScienceDirect

Biochimica et Biophysica Acta

journal homepage: www.elsevier.com/locate/bbadis

Transport and distribution of $^{45}Ca^{2+}$ in the perfused rat liver and the influence of adjuvant-induced arthritis

Karina Sayuri Utsunomiya, Luiz Guilherme Scaliante, Adelar Bracht, Emy Luiza Ishii-Iwamoto *

Laboratory of Liver Metabolism, Department of Biochemistry, University of Maringá, 87.020.900 Maringá, Brazil

ARTICLE INFO

Article history:
Received 24 April 2012
Received in revised form 30 September 2012
Accepted 6 October 2012
Available online 12 October 2012

Keywords:
Multiple-indicator dilution technique
$^{45}Ca^{2+}$ space-distribution
Rat liver
Norepinephrine
Adjuvant-induced arthritis

ABSTRACT

The purpose of the present work was to investigate Ca^{2+} transport and distribution under the conditions of the intact rat liver in health and disease (adjuvant-induced arthritis). The multiple-indicator dilution technique was used with the simultaneous injection of $^{45}Ca^{2+}$ and indicators into the portal vein under defined conditions and analysis of the outflow profiles by means of a space-distributed variable transit time model. The best description of the $^{45}Ca^{2+}$ outflow profiles corresponds to a model that assumes rapid distribution of $^{45}Ca^{2+}$ between the vascular space and the cell surface and a slower transfer into the hepatocytes. In kinetic terms two distinct cellular pools were distinguishable, the cytosol and the endoplasmic reticulum. The concentration of Ca^{2+} in the cytosol was much lower than in the vascular space and in the endoplasmic reticulum. The most prominent modification observed in the livers of arthritic rats was the increased Ca^{2+} concentration in the hormone-sensitive cellular pool. Furthermore, reduced rates of Ca^{2+} influx and efflux between the hormone-sensitive cellular pool and the cytosolic space were also detected in combination with a significantly reduced expression of the sarco-endoplasmic reticulum Ca^{2+}-ATPase (SERCA2) protein. All these observations mean that in livers from arthritic rats more time is required to replenish the hormone sensitive Ca^{2+} stores.

1. Introduction

The concentration of Ca^{2+} in the cytoplasmic space, endoplasmic reticulum, mitochondria and other intracellular organelles plays a central role in the regulation of several processes [1–5]. The long list includes glucose, fatty acid, amino acid, protein and xenobiotic metabolism, the citric acid cycle activity and ATP synthesis, bile acid and protein secretion, the movement of lysosomes and other vesicles, the cell cycle and proliferation, apoptosis and necrosis [4,5].

Alterations in cellular Ca^{2+} homeostasis and signaling have been demonstrated to produce or contribute to pathogenesis of several diseases, including diabetes [6,7], obesity [8], cardiomyopathies [9] and neurodegeneratives diseases [10]. Endoplasmic reticulum-calcium depletion in insulin-secreting cells due to changes in the ER-ATPase (SERCA), for example, seems to play a key role in beta-cell failure [11,12]. There is evidence that the proinflammatory cytokines mediate beta-cell dysfunction, acting on SERCA activity and also on mitochondrial calcium fluxes [13,7]. Although the liver is not the primary target organ in these diseases, it participates in the systemic responses, particularly in the metabolic disorders associated to diabetes and obesity and in chronic inflammatory processes such as rheumatoid arthritis (RA).

The joint is the main target of the RA but many other organs are affected and two-thirds of human patients experience a muscle wasting condition known as rheumatoid cachexia. It is believed that activated T cells stimulate B cells, monocytes, macrophages and synovial fibroblasts to produce many pro-inflammatory cytokines, prostaglandins and chemokines [14]. The pro-inflammatory mediators are released in both the local compartment, including joint or regional lymph nodes and systemic compartments (circulation and distant lymphoid tissues) [15–20]. The involvement of the liver is indicated by several metabolic changes observed in the experimental model of adjuvant-induced arthritic rats (AIA) [21,22]. Perfused livers from AIA exhibit many metabolic changes. In general terms, the catabolic pathways are stimulated and the anabolic pathways are inhibited, suggesting that the liver contributes to inflammatory cachexia [23–27]. The mechanisms implicated in these perturbations are largely unknown but the involvement of Ca^{2+} is suggested by some observations.

It is well known that a variety of channels, transporters and co-transporters located in the plasma membrane, endoplasmic reticulum and mitochondrial membranes are the elements involved in the distribution and movements of cellular Ca^{2+} in hepatocytes [2,5]. Adjuvant arthritis has been demonstrated to induce modifications in the phospholipid and fatty acid membrane composition as well as in the fluidity of microsomes, mitochondria and plasma membranes [2,28,29]. Changes in the activities of membrane-bound enzymes, including microsomal drug metabolizing enzymes [30,31] and in the glucose 6-phosphatase activity [32] were demonstrated. Strosova et al. [33] found decreased activity of SERCA associated with increased levels of protein carbonyls, decreased cysteine SH groups

* Corresponding author. Fax: +55 44 3011 4896.
E-mail address: eliiwamoto@uem.br (E.L. Ishii-Iwamoto).

0925-4439/$ – see front matter © 2012 Elsevier B.V. All rights reserved.
http://dx.doi.org/10.1016/j.bbadis.2012.10.008

and alterations in membrane fluidity of the sarcoplasmic reticulum in AIA rats. Moreover, mitochondria present greater sensitivity to the uncoupling action of Ca^{2+} [34], an effect that we have demonstrated to be consequence of the higher sensitivity of mitochondria from arthritic rats to Ca^{2+}-induced mitochondrial pore transition (MPT) [35]. All these data are indirect evidence of changes in liver Ca^{2+} homeostasis, but the influence of AIA on transport and distribution of Ca^{2+} has not yet been directly examined.

Most studies on Ca^{2+} transport and characterization of carriers and channels have been done using subcellular fractions, isolated hepatocytes and hepatocyte cell lines [36–38]. A considerable amount of knowledge has been derived from studies using these systems. However, even intact isolated hepatocytes are only partially representative of the true *in vivo* environment. For example, hepatocytes exhibit spatial polarization in their architecture, with three distinct functional regions: the basal or sinusoidal membrane facing blood in the sinusoids, the lateral membrane facing the intercellular space and the canalicular membrane [39]. This spatial polarity can be critical for the Ca^{2+} movements and distribution in the liver. Liver cell lines or isolated hepatocytes do not exhibit those features of spatial polarity. Probably, the relative distribution of many signaling proteins, including Ca^{2+} channels and hormone receptors differs considerably from that of the hepatocytes in the intact liver.

From the considerations above it seems reasonable to assume that it would be of interest to measure Ca^{2+} fluxes and distribution in the intact liver, which is exactly the purpose of the present work. Such measurements can be done by means of the multiple-indicator dilution (MID) technique, which consists in the portal injection of tracers followed by analysis of the outflow profiles. In the perfused liver both microcirculation and polarity are maintained and the kinetics of transport across the plasma membrane and the exchange between cellular pools can be assessed without disruption of the cellular integrity and without affecting bioenergetics. Essential for the successful application of the MID technique is the mathematical analysis of the dilution profiles in which the hemodynamic parameters are inferred from the outflow profiles of appropriate reference substances [40–43]. This technique has been successfully used for studying several transport phenomena in the isolated perfused rat liver under steady-state conditions [40–43]. Ca^{2+} transport, however, has not been studied through this technique until now and, thus, we have firstly studied the applicability of the experimental procedure and of the mathematical analysis to Ca^{2+} transport. In order to corroborate the reliability of the model used in the present study, experiments were also done with norepinephrine, a hormone that produces well known changes in Ca^{2+} fluxes. Finally, it is hoped that the experiments with livers from adjuvant-induced arthritic rats will reveal the potentialities of using the technique as a tool for studying the role of Ca^{2+} ions in the pathogenesis of other liver diseases.

2. Materials and methods

2.1. Materials

The liver perfusion apparatus and the rapid sampling apparatus for MID experiments were built in the workshops of the University of Maringá. $^{45}Ca^{2+}$ (1.7 mCi/mmol), [^{3}H]inulin (0.9 Ci/mmol), [^{3}H]water (20 μCi/mmol) and the biodegradable counting scintillant solution (BCS®) were purchased from Amersham Life Science (Buckinghamshire, UK). Inulin and norepinephrine were purchased from Sigma Chemical Company (St. Louis, USA). All reagent-grade chemicals were from the best available grade. Only plastic materials were used since calcium binds to glass.

2.2. Animals and induction of adjuvant arthritis

Male Holtzman rats weighing 250–300 g and fed *ad libitum* with a standard laboratory diet (Nuvilab®, São Paulo, Brazil) were used for these studies. The induction of adjuvant arthritis was done by intradermal injection of 0.1 ml of Freund's adjuvant suspension in the rat left hind paw. Freund's adjuvant is composed of inactivated and dried *Mycobacterium tuberculosis* suspended in mineral oil at a concentration of 0.5% (w/v) [44]. Experiments were performed 2 weeks after the adjuvant injection with animals presenting the typical injuries of arthritis [45].

2.3. Liver perfusion

For the surgical procedure the rats were anesthetized by intraperitoneal injection of sodium pentobarbital (50 mg kg^{-1} body weight). Hemoglobin-free, non-recirculating perfusion was performed. The surgical technique was that one described by Bracht et al. [46]. After cannulation of the portal and cava veins the liver was positioned in a Plexiglass chamber. The flow was maintained constant by a peristaltic pump (30–33 ml/min). The perfusion fluid was Krebs/Henseleit-bicarbonate buffer (pH 7.4), saturated with a mixture of oxygen and carbon dioxide (95:5) by means of a membrane oxygenator with simultaneous temperature adjustment at 37 °C. The $CaCl_2$ concentration in the perfusion fluid varied between 50 and 500 μM. The osmolarity of the perfusion fluid was compensated with NaCl. Only ultra pure water was used. When required, norepinephrine (1 μM) was dissolved in the perfusion fluid. In the experiments with norepinephrine, the portal pressure was monitored by means of an Isotec pressure transducer (Sachs Elektronik). The sensor was positioned near the entry of the portal vein. The pressure changes were computed from the recorder tracings and expressed as mm Hg. The experiments were initiated when steady-state conditions were attained as judged from the oxygen consumption rates of the livers, monitored by a Teflon-shielded platinum electrode. All experiments were approved by the Ethics Committee of Animal Experimentation of the University of Maringá.

2.4. Multiple-indicator dilution experiments

MID experiments were performed by injecting 70 μl of a mixture containing $^{45}Ca^{2+}$ (4.5 μCi), [^{3}H]inulin (4.5 μCi) and [^{3}H]water (10 μCi). In addition to labeled substances, the injected solution also contained $CaCl_2$ and inulin at concentrations equal to those in the influent perfusate. Following injection the effluent perfusate was collected in 0.5- to 2.0-s fractions over a period of 90 s following the injection by means of a specially designed fraction collector. Collection of the subsequent samples was made in 30- to 120-s intervals over a period of 1500 s. The samples were added to a biodegradable counting scintillant solution (BCS®) to measure radioactivity by liquid scintillation, with isotope discrimination for the simultaneous determination of ^{3}H (as [^{3}H]inulin and [^{3}H]water) and total $^{45}Ca^{2+}$. [^{3}H]Inulin was counted after elimination of [^{3}H]water by freeze-drying, and the latter was computed from the difference between total ^{3}H and [^{3}H]inulin. An aliquot of the injected mixture was counted for the determination of the [^{3}H]inulin to $^{45}Ca^{2+}$ ratio. From this ratio and the recovered [^{3}H]inulin (which is equal to the injected one [32]) the amount of injected $^{45}Ca^{2+}$ was calculated. All dilution curves were normalized as (amount in the effluent sample) $(s)^{-1}$ (total amount injected)$^{-1}$.

When the MID experiments were performed in the presence of norepinephrine, the injection of tracers was done at 1.5 min after starting the infusion of norepinephrine at the concentration of 1 μM, with $CaCl_2$ at the concentration of 50 μM.

2.5. Modeling $^{45}Ca^{2+}$ behavior in the perfused liver

Useful equations for the analysis of transport phenomena in the perfused liver can be derived under the assumptions of the space-distributed variable transit time model of Goresky et al. [47] plus the kinetic events underlying the possible behavior of $^{45}Ca^{2+}$ in the liver. Based on previous notions about the behavior of Ca^{2+} in the

liver a four-pool model can be devised. This model is illustrated in Fig. 1, which includes pools, movements and flow in the vascular space. The four pools are: (1) C_{e1}, the Ca^{2+} concentration in the extracellular space (the portally infused Ca^{2+}); (2) C_{e2}, which corresponds to the Ca^{2+} bound to the cell membrane and adjacencies (e.g., glycocalix); (3) C_{i1}, that represents the Ca^{2+} concentration in the first cellular pool (possibly cytosol); and (4) C_{i2}, which corresponds to the Ca^{2+} concentration in a second cellular pool (possibly organelles). It is assumed that Ca^{2+} in the extracellular space (C_{e1}) rapidly equilibrates with the cell membrane and adjacencies. The rate parameters for this equilibration are thus tending to infinity (i.e., $\lambda_1 \to \infty$ and $\lambda_2 \to \infty$), but their ratio is assumed to be finite (i.e., $\beta = \lambda_1/\lambda_2$). Exchange between the cell membrane pool (C_{e2}) and the first cellular pool (C_{i1}) is assumed to occur with transfer coefficients per unit time and unit space equal to k_1 and k_2. Similarly, k_3 and k_4 are the transfer coefficients per unit time and unit space for the exchange between the first and the second cellular pool. For the events in Fig. 1, the liver response to a single injection of $^{45}Ca^{2+}$ tracer under steady-state conditions can be described by the following equation [48,32,49]:

$$
\begin{aligned}
Q(t) = {} & Q_{\mathrm{ref}}(t)\cdot e^{-k_1(t-t_o)} + \int_0^{t-t_o} e^{-k_1\tau} Q_{\mathrm{ref}}\ (\tau + t_o)\left[e^{\alpha_1(t-t_o-\tau)} \right. \\
& \cdot \sum_{n=1}^{\infty} \frac{[k_1k_2(\alpha_1+k_4)\tau]^n (t-t_o-\tau)^{n-1}}{(\alpha_1-\alpha_2)^n n!(n-1)!} \\
& + e^{[\alpha_2(t-t_o-\tau)]} \cdot \sum_{n=1}^{\infty} \frac{[k_1k_2(\alpha_2+k_4)\tau]^n (t-t_o-\tau)^{n-1}}{(\alpha_2-\alpha_1)^n n!(n-1)!} \\
& + \int_\tau^{t-t_o} e^{\alpha_1(\varepsilon-\tau)} \sum_{n=1}^{\infty} \frac{[k_1k_2(\alpha_1+k_4)\tau]^n (\varepsilon-\tau)^{n-1}}{(\alpha_1-\alpha_2)^n n!(n-1)!} \cdot e^{[\alpha_2(t-t_o-\varepsilon)]} \\
& \left. \cdot \sum_{n=1}^{\infty} \frac{[k_1k_2(\alpha_2+k_4)\tau]^n (t-t_o-\varepsilon)^{n-1}}{(\alpha_2-\alpha_1)^n n!(n-1)!} d\varepsilon \right] d\tau
\end{aligned}
\tag{1}
$$

In Eq. (1), $Q(t)$ is the outflow profile of the injected tracer ($^{45}Ca^{2+}$), t represents time after the injection of tracer, τ the variable transit time in the sinusoids and t_0 the uniform transit time in the large vessels. The symbols α_1 and α_2 represent the roots of the quadratic equation: $s^2 + (k_2 + k_3 + k_4)s + k_2k_4 = 0$. The dimensions of the transfer coefficients are inverse time (s^{-1}), and they are referred to their corresponding distribution space (i.e., ml s^{-1} ml distribution space^{-1}). For k_1 this space corresponds to the extracellular space into which $^{45}Ca^{2+}$ undergoes flow-limited distribution and for k_2, k_3 and k_4 to the intracellular space. $Q_{\mathrm{ref}}(t)$ or $Q_{\mathrm{ref}}(\tau + t_0)$ represents the dilution curve of an appropriate reference for the whole space into which $^{45}Ca^{2+}$ undergoes flow-limited distribution. This curve can be computed from the outflow profile of [^{3}H]inulin [$Q_{\mathrm{in}}(t)$], assuming that the appropriate reference differs from [^{3}H]inulin merely because it distributes in a flow limited-fashion in an expanded space. Under this assumption, the following linear transformation can be used [50,43]:

$$
Q_{\mathrm{ref}}(t) = \frac{1}{1+\beta}\ Q_{\mathrm{in}}\left(\frac{t-t_0}{1+\beta} + t_0\right) \tag{2}
$$

According to Eq. (2), $Q_{\mathrm{ref}}(t)$ can be taken as the [^{3}H]inulin curve $Q_{\mathrm{in}}(t)$ at time $([t-t_0]/([1+\beta]+t_0)$ divided by the factor $(1+\beta)$. The parameter β is the excess extracellular space into which calcium undergoes flow-limited distribution divided by the extracellular space occupied by [^{3}H]inulin. It should be added that in the isolated perfused rat liver the [^{3}H]inulin space is practically the same as the space occupied by low molecular weight sugars such as labeled sucrose [32].

The value of t_0 was obtained from the linear superimposition of the [^{3}H]inulin curve on the [^{3}H]water curve, as predicted by Goresky [50]:

$$
Q_{\mathrm{water}}(t) = \left[\frac{1}{1+\theta}\right]\ Q_{\mathrm{in}}\left(\frac{t-t_0}{1+\theta} + t_0\right) \tag{3}
$$

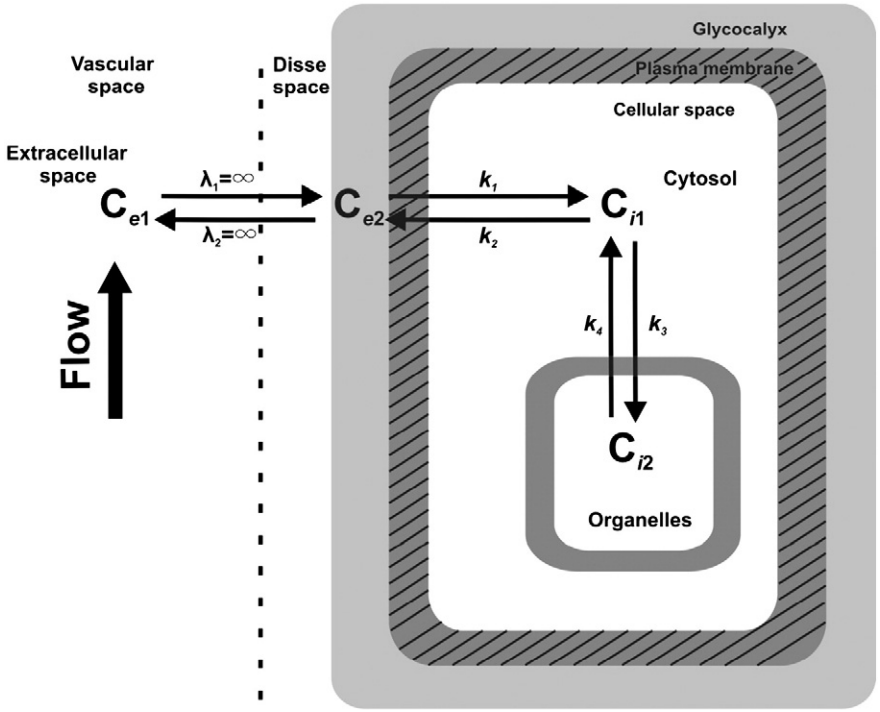

Fig. 1. Schematic representation of the events described by Eq. (1). Symbols: C_{e1}, Ca^{2+} concentration in the vascular space (extracellular space); C_{e2}, Ca^{2+} concentration in the cell membrane adjacencies; C_{i1}, Ca^{2+} concentration in the first cellular pool; C_{i2}, Ca^{2+} concentration in the second cellular pool; λ_1 and λ_2, composite transfer coefficients for the exchange between the vascular and membrane spaces; k_1 and k_2, composite transfer coefficients for the exchange between the extracellular space and the first cellular pool; k_3 and k_4, composite transfer coefficients for the exchange between the first and the second cellular pools.

The parameter θ corresponds to the ratio of intra- to extracellular water space. $Q_{water}(t)$ represents the impulse response of [^{3}H]water and $Q_{in}([t-t_0]/([1+\theta]+t_0)$ corresponds to the [^{3}H]inulin curve at time $([t-t_0]/([1+\theta]+t_0)$. Eq. (3) assumes flow-limited distribution of both tracers.

The mean transit time of tracers ($\bar{t}$) was calculated according to Meier and Zierler [51]:

$$\bar{t} = \int_0^\infty Q(t)\cdot t \; dt \tag{4}$$

$Q(t)$ represents the normalized curve of the tracer and t represents time after injection.

2.6. Pool sizes and exchange rates

Pool sizes and exchange rates can be calculated from the transfer coefficients and the extracellular Ca^{2+} concentration (C_{e1}). The pool that exchanges rapidly with the extracellular space (C_{e2}) can be calculated as:

$$C_{e2} = C_{e1} \times \beta \tag{5}$$

C_{e2} has the dimensions of nmol $Ca^{2+}\times$(ml extracellular reference space)$^{-1}$. The extracellular reference space differs from the extracellular water space by the factor $(1+\beta)$.

Under the steady-state conditions maintained by the continuous infusion of non-radioactive Ca^{2+} into the perfusion fluid and in the absence of net fluxes across the barriers (membranes) limiting the cellular pools, the rates of influx are equal to the rates of efflux. Under the assumption that the extracellular Ca^{2+} pool (C_{e1}) is in equilibrium with Ca^{2+} bound to the cell membrane and adjacencies, the exchange rate across the cell membrane ($F_1^{i\leftrightarrow e}$) can be calculated as:

$$F_1^{i\leftrightarrow e} = \frac{k_1}{\theta/(1+\beta)} \times C_{e1} = k_2 \times C_{i1}. \tag{6}$$

Since C_{e1} corresponds to the known portal Ca^{2+} concentration, C_{i1} can be calculated as:

$$C_{i1} = C_{e1} \times \frac{k_1}{k_2}\left[\frac{1}{\theta/(1+\beta)}\right] = \frac{F_1^{i\leftrightarrow e}}{k_2}. \tag{7}$$

Similarly, the exchange rate between the first and the second cellular pools ($F_2^{i\leftrightarrow e}$) is given by:

$$F_2^{i\leftrightarrow e} = k_3 \times C_{i1} = k_4 \times C_{i2}. \tag{8}$$

If C_{i1} is calculated previously using Eq. (7), C_{i2} can be calculated as:

$$C_{i2} = \frac{k_3}{k_4} \times C_{i1} = \frac{F_2^{i\leftrightarrow e}}{k_4}. \tag{9}$$

When calculated according to Eqs. (6) and (8), the exchange rates are referred to the aqueous cell space of the liver. They have the dimensions of nmol $Ca^{2+}\times s^{-1}\times$(ml total intracellular aqueous space accessible to [^{3}H]water)$^{-1}$.

2.7. Calculations

The first step was to obtain the transit time in the large vessels (t_0) by means of an optimized superimposition of the [^{3}H]water and [^{3}H]inulin curves according to Eq. (3). A nonlinear iterative least-squares procedure was used [30]. In the next step Eqs. (1) and (2) were fitted simultaneously to the experimental outflow profiles of $^{45}Ca^{2+}$ together with the previously optimized value of t_0 and provisional estimates of β, k_1, k_2, k_3 and k_4. Iterations of the nonlinear least-squares procedures were continued until the standard deviation of the estimate was minimized. The integrals in Eq. (1) were calculated by the Romberg's algorithm [30]. Interpolations were done using Stineman's interpolation formula [52]. The integrals in Eq. (4) (mean transit time) were determined by means of the trapezoid rule with monoexponential extrapolation to infinity [51].

2.8. Quantitative polymerase chain reaction

Total RNA was isolated from livers of control and arthritic rats using the Trizol reagent (Invitrogen, Breda, The Netherlands). cDNA was synthesized from total RNA with an oligo-dT12-18 primer and Superscript III reverse transcriptase (Invitrogen). Real-time PCR measurements were performed at 60 °C in a Light Cycler 480 apparatus (Roche, Mannheim, Germany) with Light Cycler Fast start DNA Master Plus SYBR Green I (Roche). The mRNA level of SERCA2 was normalized to 18S rRNA.

The primer sequences are as follows: 18S rRNA: 5′-gggaggtagt gacgaaaaataacaat-3′ and 3′-ttgccctccaatggatcct-5′; SERCA 2: 5′-tctgtca ttcgggagtgggg-3′ and 3′-gcaccaccaactgcttagcc-5′.

2.9. Treatment of data

The data in tables and figures were expressed as mean ± standard error (SE). The statistical significance of the differences between parameters was evaluated by Student's *t*-test or by means of one-way ANOVA with significant differences among means identified by Newman–Keuls' testing. The results were reported as probability values, the criterion of significance being $P<0.05$. Statistical analysis was performed by means of the Statistica or GraphPad Software. Linear and nonlinear regression analysis was done by means of GraphPad Software.

3. Results

3.1. Typical outflow profiles of $^{45}Ca^{2+}$ and indicators in livers from normal rats

Fig. 2 shows four typical outflow profiles of experiments in which $^{45}Ca^{2+}$, [^{3}H]inulin and [^{3}H]water were injected. They were obtained with four $CaCl_2$ concentrations in the perfusion fluid: 50 μM (panel A), 100 μM (panel B), 250 μM (panel C) and 500 μM (panel D). All curves were normalized by dividing the amount of radioactivity that reappeared per second by the total injected radioactivity. If there is no loss within the liver, the areas under such normalized curves are equal to unity. This occurred with all $^{45}Ca^{2+}$ curves obtained in the present work denoting that there was no loss or sequestration of label. As expected, the [^{3}H]water outflow profile was delayed in relation to the [^{3}H]inulin outflow profile because water distributes over the entire aqueous space of the liver, whereas [^{3}H]inulin does not exchange with the cellular space during a single passage. At 50 μM $CaCl_2$ (panel A), the outflow profile of $^{45}Ca^{2+}$ had an initial upslope that was slightly delayed with respect to that of [^{3}H]inulin profile and reached a lower magnitude. Furthermore, the peak time of the $^{45}Ca^{2+}$ curve was slightly shifted to the right and its downslope decayed more slowly in relation to the [^{3}H]inulin curve, so that both curves crossed soon after the peak time.

When the $CaCl_2$ concentration was increased from 50 to 100 μM (panel B), 250 μM (panel C) and 500 μM (panel D), the $^{45}Ca^{2+}$ outflow profiles progressively approached those of [^{3}H]inulin. Differences in the peak values progressively diminished as the $CaCl_2$ concentration increased, as well as the differences that were observed in the downslope of the $^{45}Ca^{2+}$ and [^{3}H]inulin outflow profiles at the 50 μM concentration (panel A). These findings are characteristic of saturation phenomena.

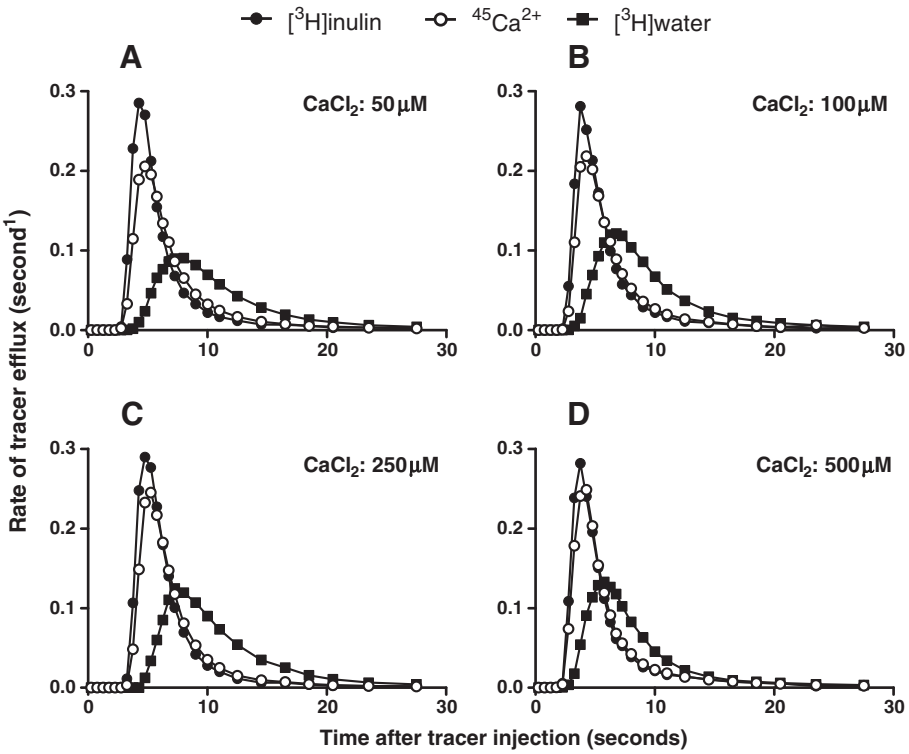

Fig. 2. Typical outflow profiles of $^{45}Ca^{2+}$ and indicator substances at various $CaCl_2$ concentrations in the perfusion fluid. Livers from fed rats were perfused in an open system with Krebs/Henseleit-bicarbonate buffer (pH 7.4) containing 1 mM inulin and 50 μM (A), 100 μM (B), 250 μM (C) or 500 μM (D) $CaCl_2$, as indicated on each graph. After oxygen consumption stabilization, trace amounts of [^{3}H]inulin (●—●), $^{45}Ca^{2+}$ (○—○) and [^{3}H]water (■—■) were injected simultaneously into the portal vein. The outflowing perfusate was fractionated, and the radioactivity in each sample was evaluated by means of isotope discrimination. Fractions of the injected radioactivity of each component appearing in the effluent perfusate per second are represented against the time after injection. The curves in panels A, B, C and D are representative of 6, 7, 6 and 4 indicator-dilution experiments, respectively.

3.2. Model analysis of the outflow profiles of $^{45}Ca^{2+}$

The transfer coefficients in the scheme of Fig. 1 can be obtained by fitting Eqs. (1) and (2) to the experimental data. If the equations fit to the experimental data, this can be taken as a first indication that the model in Fig. 1 in fact describes the main events that follow a bolus injection of $^{45}Ca^{2+}$. Despite the small differences between the [^{3}H]inulin and $^{45}Ca^{2+}$ outflow profiles at the highest $CaCl_2$ concentrations in the perfusion fluid, Eq. (1) could be fitted to all $^{45}Ca^{2+}$ outflow profiles. Examples are shown in Fig. 3, which illustrates results of the calculations with experiments of the kind shown in Fig. 2. The closed circles represent the experimental data and the solid lines the calculated curves. The optimized parameters are given on each graph. There was a good agreement between theory and experiment. Similar good fits were obtained for all experiments at various $CaCl_2$ concentrations. The traced line in Fig. 3 is the curve of the new reference $Q_{ref}(t)$, as given by Eq. (2). The curves of the new reference differ from those of [^{3}H]inulin shown in Fig. 2 because of an extra, apparent or real, extracellular space into which $^{45}Ca^{2+}$ undergoes flow-limited distribution, but from which [^{3}H]inulin is excluded. This $^{45}Ca^{2+}$ distribution space exceeds that of [^{3}H]inulin by a relatively small factor, given by $(1+\beta)$. The parameter β was equal to 0.12 ± 0.008 at 50 μM extracellular Ca^{2+}. As the extracellular $CaCl_2$ concentration was increased to 100, 250 and 500 μM, the values of β slightly decreased to 0.11 ± 0.008, 0.093 ± 0.007 and 0.099 ± 0.006, respectively.

Eq. (1) allows the resolution of the calculated $^{45}Ca^{2+}$ outflow profiles into the throughput and exchanged components. The throughput comprises the fraction of the injected $^{45}Ca^{2+}$ which did not enter the cellular space and traveled to the outflow in the same manner as the new reference. The second component (exchanged) corresponds to the fraction that entered the cells at least once. These two components are given by the first (throughput) and the second, and more complex term (exchanged), in Eq. (1). Fig. 4 illustrates these separable components of the same set of curves shown in Fig. 3. The fractions of $^{45}Ca^{2+}$ that entered the liver and returned to the perfusate were the smallest components of the curves. The mean values of the exchanged components passed from 25.3% at 50 μM $CaCl_2$ to 17.1%, 17.1% and 7.7% at 100, 250 and 500 μM, respectively.

Several transport parameters were derived from the fitting procedures of Eq. (1) to the experimental data. In general, all transfer coefficients could be optimized excepting k_3 and k_4 in the experimental series with 500 μM $CaCl_2$. At this concentration, the fraction of tracer ($^{45}Ca^{2+}$) that entered the cells (exchanged) was minimal as shown in Fig. 4 (panel D) and the outflow profile contained not enough information for determining k_3 and k_4. This is also why experiments were not done at $CaCl_2$ concentrations higher than 500 μM.

Fig. 5 shows the changes in the transfer coefficients with increasing $CaCl_2$ concentrations in the perfusion fluid (extracellular space). Comparison of the values estimated at 50 μM reveals that the transfer coefficient for Ca^{2+} efflux from the first intracellular space (k_2) was substantially higher than the transfer coefficient for Ca^{2+} entry into the cells (k_1). On the other hand, the transfer coefficient for Ca^{2+} entry into the second cellular pool (k_3) was significantly higher than the value for Ca^{2+} efflux from this pool (k_4).

The transfer coefficients k_1 and k_2 (panel A) showed a clear dependence on the extracellular $CaCl_2$ concentration (C_{e1}). They decreased progressively as C_{e1} increased. The same trend was seen with the transfer coefficients for influx into the second intracellular pool (k_3) (panel B). The transfer coefficients for efflux (k_4), however, were not dependent of the $CaCl_2$ concentration in the range between 50 and 250 μM.

The progressive decrease in k_1 and k_2 when the extracellular Ca^{2+} concentration was increased reflects most probably saturation of the

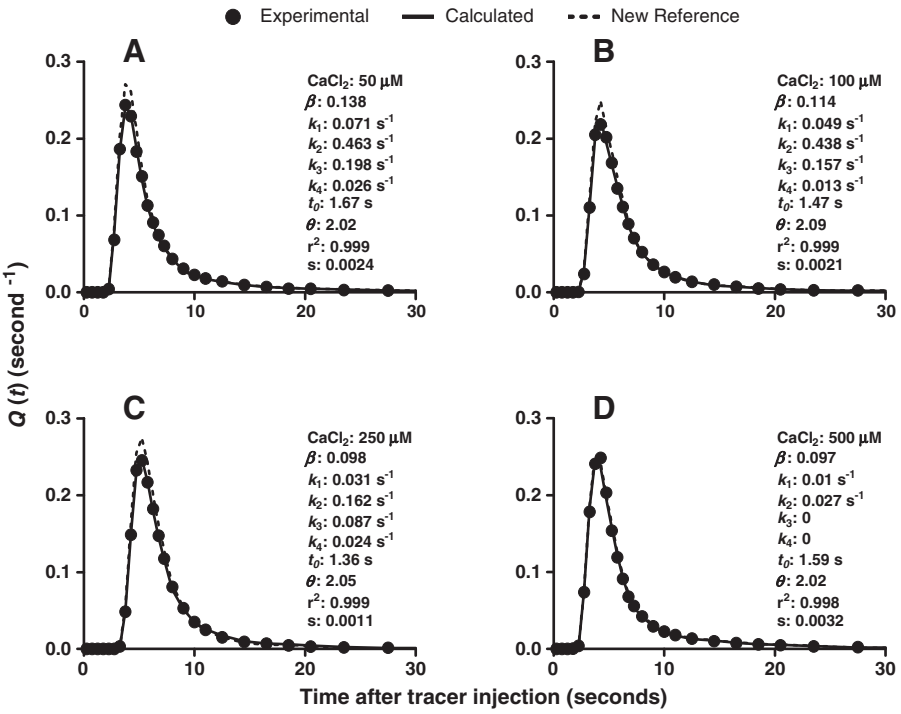

Fig. 3. Model analysis of four typical outflow profiles of $^{45}Ca^{2+}$. Eq. (1) was fitted to the experimental outflow profiles of $^{45}Ca^{2+}$ obtained in the presence of variable $CaCl_2$ concentrations in the perfusion fluid. Fitting was performed as described in Materials and methods. The experimental conditions and the optimized values of the various parameters are listed in each graph, together with the standard error of the estimate(s) and the coefficient of determination (r^2). The optimized values of t_0 and θ were obtained from a linear superimposition of the [^{3}H]water and [^{3}H]inulin curves, according to Eq. (3). The reference curve was generated from the [^{3}H]inulin curve according to Eq. (2). Key: ●, experimental dilution curve of $^{45}Ca^{2+}$; —, calculated curve employing the optimized parameters; - - -, computed reference curve [$Q_{ref}(t)$]. The curves in panels A, B, C and D are representative of 6, 7, 6 and 4 indicator dilution experiments, respectively.

carrier-mediated transfer systems between the vascular space and the first cellular pool. Saturation of Ca^{2+} influx from the first into the second cellular pool was also indicated by the decrease in k_3. It was also apparent that the transfer of Ca^{2+} across the plasma membrane saturates at lower vascular Ca^{2+} concentrations than the transfer of Ca^{2+} into the second cellular pool.

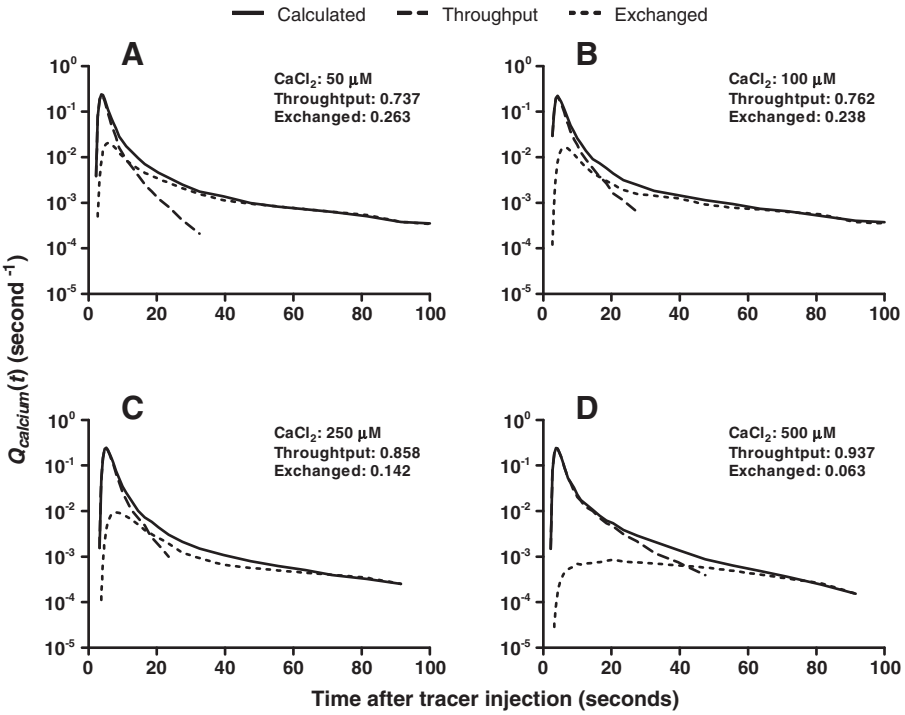

Fig. 4. Resolution of the theoretical outflow profiles of $^{45}Ca^{2+}$ into their components, throughput and exchanged. The continuous lines represent the calculated curves of the same experiments shown in Fig. 3 plotted on a logarithmic scale *versus* time following injection. The values given on each graph represent the fractions of total injected $^{45}Ca^{2+}$ which entered (exchanged) or did not enter the cellular space (throughput).

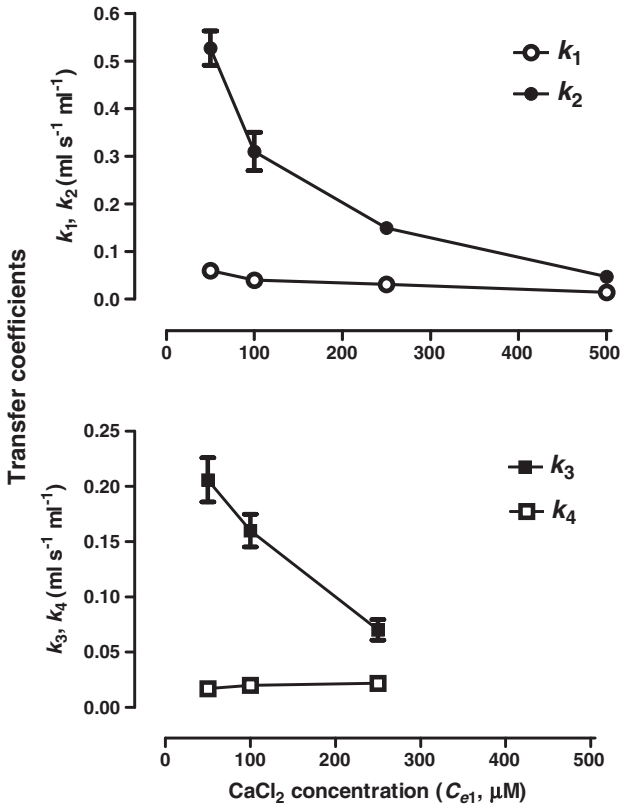

Fig. 5. Changes in the transfer coefficients of $^{45}Ca^{2+}$ as a function of the $CaCl_2$ concentration in the perfusion fluid (C_{e1}). The mean transfer coefficients were obtained by fitting Eqs. (1) and (2) to the experimental outflow profiles. The data points represent the mean of four to seven liver perfusion experiments. Vertical bars are standard errors.

3.3. Pool sizes and exchange rates of $^{45}Ca^{2+}$

The pool sizes C_{e2}, C_{i1} and C_{i2} were calculated according to Eqs. (5), (7) and (9), respectively. In Fig. 6 C_{e2} was plotted against C_{e1}. The relation was linear over the concentration range of the present experiments, the pertinent coefficient of determination (r^2) being equal to 0.9964. This linear relationship indicates a single partition coefficient for the distribution of Ca^{2+} between the vascular space and the cell membrane pool.

Fig. 7 shows a representation of C_{i1} against C_{e1} and Table 1 lists the C_{i1}/C_{e1} ratios for each C_{e1} value. The relation between C_{i1} and C_{e1} was clearly parabolic. The C_{i1}/C_{e1} ratios (Table 1) were smaller than unity, as expected from previous notions about the strong concentration gradient between the vascular and cytosolic spaces. At C_{e1} equal to 50 µM, the Ca^{2+} concentration in the first cellular pool was nearly one order of magnitude lower.

The relation between C_{i2} and C_{i1} (Fig. 8) is hyperbolic. In agreement with the widespread notion about the existence of highly concentrated intracellular Ca^{2+} pools (endoplasmic reticulum and mitochondria), the calculations revealed a large concentration gradient between the first (C_{i1}) and the second cellular (C_{i2}) pools (Table 1). At the portal concentration of 50 µM, C_{i2} was 14.6 fold higher than C_{i1}. Contrasting with the C_{i1}/C_{e1} values, the C_{i2}/C_{i1} ratio diminished when the portal Ca^{2+} concentration was raised.

Fig. 9 illustrates the relation between the exchange rates $F_1^{i\leftrightarrow e}$ and $F_2^{i\leftrightarrow e}$ and the corresponding concentrations C_{e1} and C_{i1}. A quantitative analysis of the correlation between the parameters is difficult because of the low number of experimental points, specially for $F_2^{i\leftrightarrow e}$, but it seems clear they both are saturable functions of the concentrations in the corresponding spaces. The classical Michaelis–Menten equation was fitted to the $F_1^{i\leftrightarrow e}$ *versus* C_{e1} (i.e., $F_1^{i\leftrightarrow e} = V_{max}C_{e1}/(K_M + C_{e1})$) and

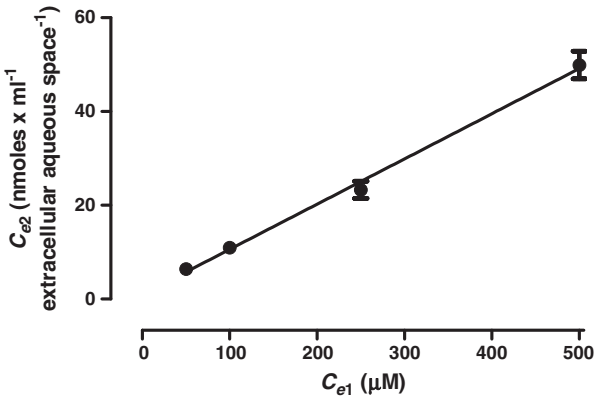

Fig. 6. Concentration of Ca^{2+} in the cell membrane (C_{e2}) as a function of the concentration in the vascular space (C_{e1}). The C_{e2} values were calculated from β and C_{e1}, employing Eq. (5). β was obtained by fitting Eqs. (1) and (2) to the outflow profiles. The data points represent the mean of four to seven liver perfusion experiments. Vertical bars are standard errors. The continuous line is the regression line, calculated as $y = 0.096x + 0.958$. The coefficient of determination (r^2) is equal to 0.996.

$F_2^{i\leftrightarrow e}$ *versus* C_{i1} (i.e., $F_2^{i\leftrightarrow e} = V_{max}C_{i1}/(K_M + C_{i1})$) relationships. The equation accounted reasonably well for both experimental curves even though the $F_1^{i\leftrightarrow e}$ *versus* C_{e1} relationship presented considerable dispersion. The K_M for the exchange between the extracellular space and the first cellular pool ($F_1^{i\leftrightarrow e}$) was equal to 124.5 ± 60.62 µM, and the V_{max} 5.16 ± 0.98 nmol s^{-1} ml^{-1}. The corresponding values for the exchange between the first and second cellular pools ($F_2^{i\leftrightarrow e}$) were 9.38 ± 3.21 µM and 2.42 ± 0.34 nmol s^{-1} ml^{-1}, respectively.

3.4. The influence of norepinephrine on transfer coefficients and distribution space of Ca^{2+}

The second Ca^{2+} pool revealed by the analysis of the MID experiments does not necessarily correspond to a single anatomical compartment, for example, endoplasmic reticulum or mitochondria. It may also be representing a group of pools that can not be distinguished by kinetic means. The use of agents that modify Ca^{2+} fluxes by known mechanisms can be helpful in the identification of the second compartment. One such agent is norepinephrine, which is known to modify several Ca^{2+} fluxes, to trigger mobilization of the calcium stores in the endoplasmic reticulum and to increase the cytosolic calcium concentration [1,4,5]. For this reason the MID experiments were

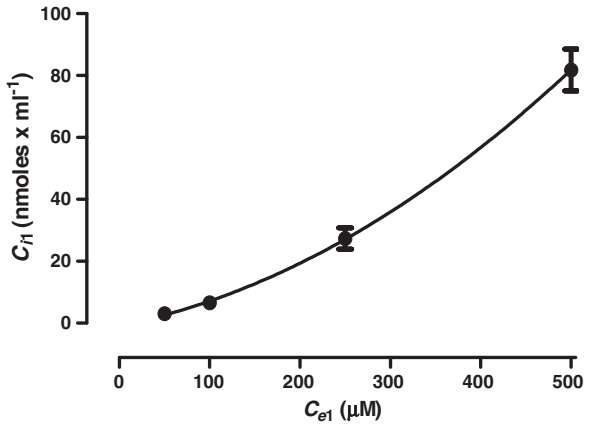

Fig. 7. Concentration of Ca^{2+} in the first cellular pool (C_{i1}) as a function of the concentration in the vascular space (C_{e1}). The C_{i1} values were calculated employing Eq. (7). The transfer coefficients were derived by fitting Eqs. (1) and (2) to the outflow profiles. The data points represent the mean of four to seven liver perfusion experiments. Vertical bars are standard errors. The continuous line is the regression curve, calculated as $y = 2.39 + 0.024x + 0.0008x^2 - (4.84\ 10^{-7})x^3$. The coefficient of determination (r^2) is equal to 0.991.

Table 1
Ca^{2+} concentration ratios as a function of the extracellular calcium concentration. The concentrations of Ca^{2+} in the first (C_{i1}) and second (C_{i2}) cellular pools were calculated according to Eqs. (7) and (9). Significant differences between means are identified by pairs of letters in each column, as determined by ANOVA with Newman–Keuls' testing ($P<0.05$).

Extracellular $CaCl_2$ concentration (C_{e1}) μM	C_{i1}/C_{e1}	C_{i2}/C_{i1}
50 ($n=6$)	0.062 ± 0.0078^{a}	14.62 ± 3.72^{a}
100 ($n=7$)	0.070 ± 0.012^{b}	9.49 ± 0.96
250 ($n=6$)	$0.109 \pm 0.0135^{a,b,c}$	3.27 ± 0.37^{a}
500 ($n=4$)	$0.164 \pm 0.0135^{a,b,c}$	–

performed with norepinephrine in the perfusion fluid. The injection of tracers was done at 1.5 min after starting the infusion of norepinephrine at the concentration of 1 μM, with $CaCl_2$ at the concentration of 50 μM. At this time, norepinephrine was found to induce the maximal increase in the portal pressure under the same experimental conditions as the indicator dilution experiments. The increment reached 1.5 mm Hg relative to the basal pressure (data not shown). At the injection time of 1.5 min following the onset of norepinephrine infusion, a transient net efflux of Ca^{2+} from the cytosol will be occurring [1]. This net efflux corresponds to a transition between different steady-state conditions, thus invalidating Eqs. (5) to (9), which can not be used for calculating pool sizes in the presence of norepinephrine.

As revealed by Table 2, norepinephrine infusion in livers from normal rats increased the vascular space (V_e) accessible to labeled inulin by 24% and increased the accessible cellular space (V_i) by 35%. The ratio of V_i to V_e (θ), however, was not modified. Norepinephrine did not modify the volume of the non-exchanging vessels as t_0 was not significantly modified. The throughput and exchanged components of the calculated $^{45}Ca^{2+}$ outflow profile were also not modified by norepinephrine. Norepinephrine infusion, however, caused substantial alterations in the transfer coefficients. The transfer coefficient for efflux from the cytosolic pool to the extracellular space (k_2) was 70% lower than that for the control condition. The values of k_1 were not altered, although a tendency toward smaller values was apparent. The k_2/k_1 ratio was reduced from 10.02 (control) to 4.38.

The most prominent effect of norepinephrine was on the transfer coefficient for efflux from the second pool (k_4), which was 188% increased. In opposition, the transfer coefficient for Ca^{2+} influx into the second compartment (k_3) was 30% reduced. The combination of these opposite effects led to a strong diminution of the k_3/k_4 ratio. It was equal to 14.6 in the control condition and reduced to 3.4 in the presence of norepinephrine. In general it can be said that the modifications caused by norepinephrine are those expected if one takes into account previous notions about the action of this hormone [1,4,5].

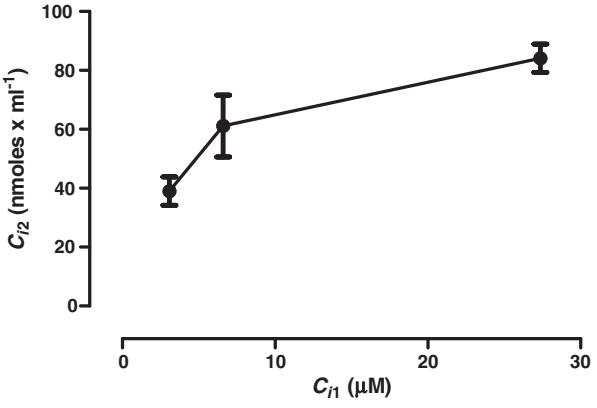

Fig. 8. Concentration of Ca^{2+} in the second cellular pool (C_{i2}) as a function of the concentration in the first cellular pool (C_{i1}). C_{i1} values were calculated employing Eq. (7). The C_{i2} values were calculated employing Eq. (9). The transfer coefficients were derived by fitting Eqs. (1) and (2) to the outflow profiles. The data points represent the means of six to seven liver perfusion experiments. Vertical bars are standard errors.

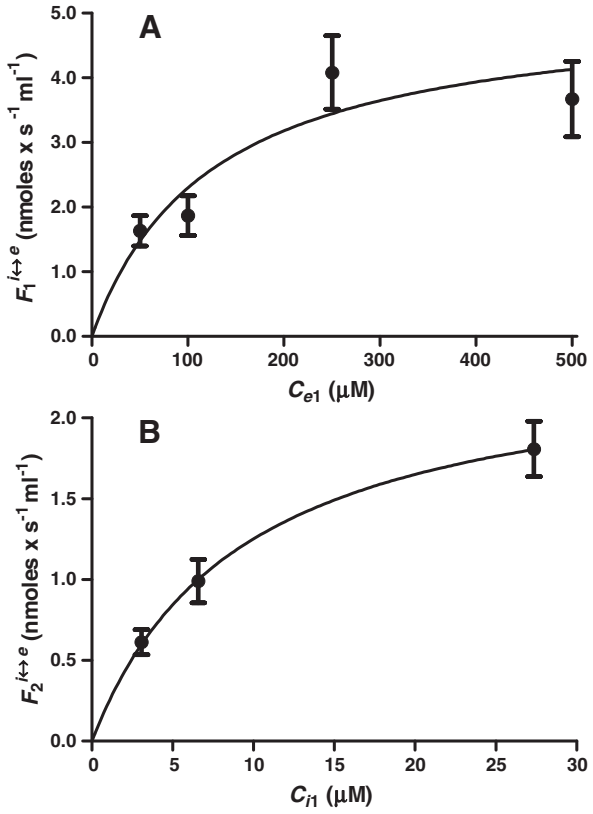

Fig. 9. Concentration dependences of the rates of Ca^{2+} exchange. A: exchange between the extracellular space and the first cellular pool ($F_1^{i\leftrightarrow e}$ *versus* C_{e1}). B: exchange between the first cellular pool and the second cellular pool ($F_2^{i\leftrightarrow e}$ *versus* C_{i1}). Rates were calculated according to Eqs. (6) ($F_1^{i\leftrightarrow e}$) and (8) ($F_2^{i\leftrightarrow e}$) using the rate constants derived by fitting Eqs. (1) and (2) to the outflow profiles. C_{i1} was calculated according to Eq. (7). The data points represent the mean of four to seven liver perfusion experiments. Vertical bars are standard errors. The continuous lines joining the experimental data are the nonlinear regression curves calculated with the fitted Michaelis–Menten equation ($F_1^{i\leftrightarrow e} = V_{max} \times C_{e1}/(K_M + C_{e1})$ and $F_2^{i\leftrightarrow e} = V_{max} \times C_{i1}/(K_M + C_{i1})$).

3.5. The influence of adjuvant-induced arthritis on the transfer coefficients and distribution space of Ca^{2+}

Dilution experiments with livers from adjuvant induced arthritic rats were performed in the absence or presence of 1 μM norepinephrine. The experimental protocol was the same as that one used in livers from normal rats, as illustrated by Fig. 2A, and the extracellular Ca^{2+} concentration was 50 μM. Fig. 10A shows typical outflow profiles of $^{45}Ca^{2+}$, [^{3}H]inulin and [^{3}H]water obtained with a liver from an arthritic rat in the absence of norepinephrine. Panel B shows the $^{45}Ca^{2+}$ theoretical curve obtained by fitting Eq. (1) to the experimental data, the optimized parameters and the computed reference curve ($Q_{ref}(t)$), as given by Eq. (2). The resolution of the calculated $^{45}Ca^{2+}$ outflow profile into the throughput and exchanged components is shown in panel C. The agreement between the calculated and experimental curves of $^{45}Ca^{2+}$ in livers from arthritic rats is comparable to that found in livers from normal rats. The parameters that were obtained from the fitting procedures are listed in Table 2 and Fig. 11, and they reveal that arthritis caused modifications in Ca^{2+} transport as well as in other parameters. Arthritis caused a reduction of 17% in t_0 (large vessels transit time) and an increase of approximately 30% in V_e and V_i when compared to the control condition. The parameters V_i/V_e, θ and β, however, were not significantly modified. The modifications in the transfer

Table 2
Effects of 1 μM norepinephrine on parameters of transport and distribution of $^{45}Ca^{2+}$ in livers from normal and arthritic rats. All parameters were obtained from multiple-indicator dilution experiments performed with 50 μM $CaCl_2$ in the perfusion fluid as those illustrated by Figs. 2A and 10A. The parameters were obtained by fitting Eqs. (1) and (2) to the experimental outflow profiles. In the norepinephrine experimental series the injection of tracers was done 1.5 min after the onset of the hormone infusion. The data are means ± SE. Significant differences between means are identified by pairs of identical symbols in each row as determined by means of Student's *t*-test ($P<0.05$).

Parameter	Normal rats		Arthritic rats	
	Control ($n=6$)	Norepinephrine ($n=5$)	Control ($n=4$)	Norepinephrine ($n=6$)
t_0 (s)	$1.64\pm0.062^{\#}$	1.49 ± 0.0723	$1.352\pm0.049^{\#}$ (−17%)	1.376 ± 0.053
θ	2.041 ± 0.069	2.203 ± 0.0267	2.043 ± 0.014	2.072 ± 0.022
V_e as flow × $(\bar{t}_{in}-t_0)$ (ml/g)	$0.233\pm0.01^{*,\#}$	$0.29\pm0.018^{*}$ (+24%)	$0.31\pm0.015^{\#}$ (+32%)	0.291 ± 0.021
V_i as flow × $(\bar{t}_w-\bar{t}_{in})$ (ml/g)	$0.482\pm0.021^{*,\#}$	$0.648\pm0.029^{*}$ (+34%)	$0.642\pm0.021^{\#}$ (+33%)	0.618 ± 0.042
V_i as flow × $(\bar{t}_{in}-t_0)\times\theta$ (ml/g)	$0.473\pm0.02^{*,\#}$	$0.639\pm0.036^{*}$ (+35%)	$0.621\pm0.028^{\#}$ (+31%)	0.602 ± 0.043
V_i/V_e	2.076 ± 0.045	2.246 ± 0.071	2.097 ± 0.043	2.13 ± 0.024
β	0.128 ± 0.008	0.097 ± 0.0182	0.103 ± 0.021	0.100 ± 0.021
k_1 (s^{-1})	0.059 ± 0.009	0.038 ± 0.007	0.095 ± 0.027	0.059 ± 0.005
k_2 (s^{-1})	$0.527\pm0.036^{*}$	$0.155\pm0.0168^{*}$ (−70%)	$0.61\pm0.146^{\ddagger}$	$0.269\pm0.023^{\ddagger}$ (−56%)
k_3 (s^{-1})	$0.206\pm0.020^{*,\#}$	$0.144\pm0.014^{*}$ (−30%)	$0.135\pm0.009^{\#}$ (−34%)	0.111 ± 0.015
k_4 (s^{-1})	$0.017\pm0.003^{*,\#}$	$0.049\pm0.013^{*}$ (+188%)	$0.005\pm0.001^{\#,\ddagger}$ (−70%)	$0.014\pm0.002^{\ddagger}$ (+180%)
k_2/k_1	$10.02\pm1.6^{*}$	$4.38\pm0.51^{*}$ (−56%)	$6.85\pm0.98^{\ddagger}$	$4.6\pm0.22^{\ddagger}$ (−33%)
k_3/k_4	$14.62\pm3.72^{*,\#}$	$3.44\pm0.54^{*}$ (−76%)	$30.39\pm5.36^{\#,\ddagger}$ (+108%)	$8.22\pm1.14^{\ddagger}$ (−73%)
Throughput	$0.747\pm0.025^{\#}$	0.758 ± 0.04	$0.63\pm0.026^{\#}$ (−16%)	0.666 ± 0.017
Exchanged	$0.253\pm0.025^{\#}$	0.242 ± 0.04	$0.37\pm0.026^{\#}$ (+46%)	0.334 ± 0.017

Symbols: $^{\#}$normal control *versus* arthritic control; *normal control *versus* normal norepinephrine; ‡arthritic control *versus* arthritic norepinephrine.

coefficients for Ca^{2+} exchange between the extracellular space and the first cellular pool (k_1 and k_2) were not entirely clear but a strong tendency toward higher values of k_1 ($P=0.17$) was apparent without modification in k_2. This increasing tendency for k_1 was confirmed by the significant increment (+46%) in the exchanged component of the Ca^{2+} outflow profile. This increment also means an increased rate of exchange between the extracellular space and the first cellular pool ($F_1^{i\leftrightarrow e}$) of approximately 114% (Fig. 11A). On the other hand, arthritis produced significant diminutions in the transfer coefficients for Ca^{2+} exchange between the first and second cellular pools (k_3 and k_4). In relative terms, the reduction in k_4 (efflux; −70%) was more pronounced than that in k_3 (influx; −34%). The steady-state rates of exchange between the first and second cellular pools ($F_2^{i\leftrightarrow e}$), however, were not modified.

Eqs. (5) to (9) were again used to calculate pool concentrations. Fig. 11B reveals that arthritis did not change the Ca^{2+} concentration in the rapid exchanging extracellular pool (C_{e2}) and in the first cellular pool (C_{i1}). An increase occurred, however, in the concentration of the second cellular pool (C_{i2}). In consequence, the concentration gradient between the second and the first cellular pool was also considerably increased from 14.6 ± 3.7 (Table 1) to 30.4 ± 5.4. This reflects the fact that arthritis diminished much more the transfer coefficient for efflux (k_4) than the transfer coefficient for influx (k_3), as shown in Table 2.

Data in Table 2 also show that the responses of livers from arthritic rats to norepinephrine infusion were similar but not exactly the same as those observed in livers from normal rats. The most striking difference was the lack of change in the transfer coefficient k_3, contrasting with the diminution observed in the normal condition. Similarly to the normal condition, on the other hand, the coefficient for Ca^{2+} efflux from the first cytosolic pool (k_2) was diminished (−56%), the transfer coefficient for Ca^{2+} efflux from the second cellular pool (k_4) was increased (+180%), and the values of k_1 were not significantly modified. Due to the lack of change in the transfer coefficient k_3, the k_3/k_4 ratio, which was 3.4 in livers from normal rats, increased to 8.2 in livers from arthritic rats (Table 2). Another useful comparison are the changes caused by norepinephrine in the transfer coefficient k_4 (efflux from the second cellular pool) in the normal and arthritic condition. In both cases k_4 was increased by norepinephrine by the same factor of 2.8.

3.6. The influence of adjuvant-induced arthritis on the expression of SERCA2 in livers.

Fig. 12 shows the mRNA levels of SERCA2 normalized to 18S rRNA in livers from normal and adjuvant-induced arthritic rats. The expression of SERCA2 was approximately 2.8 times lower in livers from arthritic rats when compared to the control livers.

4. Discussion

4.1. General considerations

In the present work we have shown that the overall behavior of Ca^{2+} can be analyzed in the perfused liver by means of the MID technique. This behavior conforms to the generally accepted notions about the compartmentation of Ca^{2+} and its role as an intracellular messenger. The most important requisite for using the MID technique in studies regarding modifications in hepatic calcium homeostasis is in agreement between theory and experiment. The successful fitting of Eq. (1) to practically all outflow profiles obtained in the present work under various conditions represents the most important fulfillment of this requisite. The consistency of the parameters that were obtained, however, is equally important. For example, various expected concentration gradients were found and these were modified by norepinephrine in a way that can be predicted based on previous knowledge. Furthermore, positive correlations between exchange rates and concentrations were also found. Such correlations were saturable functions, as expected from carrier mediated processes.

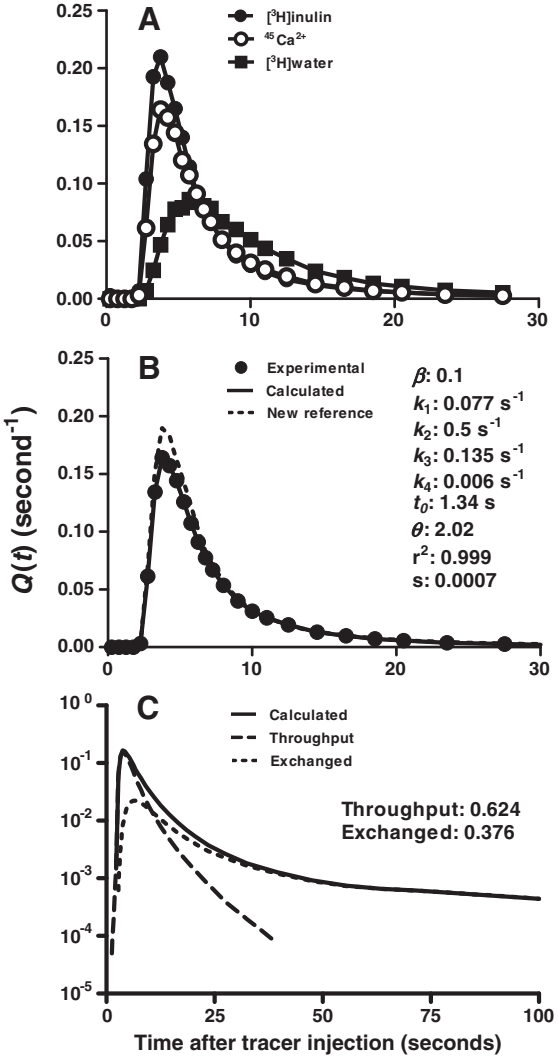

Fig. 10. Typical outflow profiles of $^{45}Ca^{2+}$ and indicators obtained with a liver from an adjuvant-induced arthritic rat. The liver was perfused with Krebs/Henseleit-bicarbonate buffer (pH 7.4) containing 1 mM inulin and 50 μM $CaCl_2$. A: experimental outflow profiles of [^{3}H]inulin (●—●), $^{45}Ca^{2+}$ (○—○) and [^{3}H]water (■—■). B: calculated (Eq. (1), —) and experimental (●) $^{45}Ca^{2+}$ curves and the new reference (Eq. (2), ·····). C: resolution of the theoretical outflow profile of $^{45}Ca^{2+}$ (—) into its components, throughput (— — —) and exchanged (·····) plotted on a logarithmic scale *versus* time following injection. All parameters were obtained by fitting Eqs. (1) and (2) to the experimental outflow profiles.

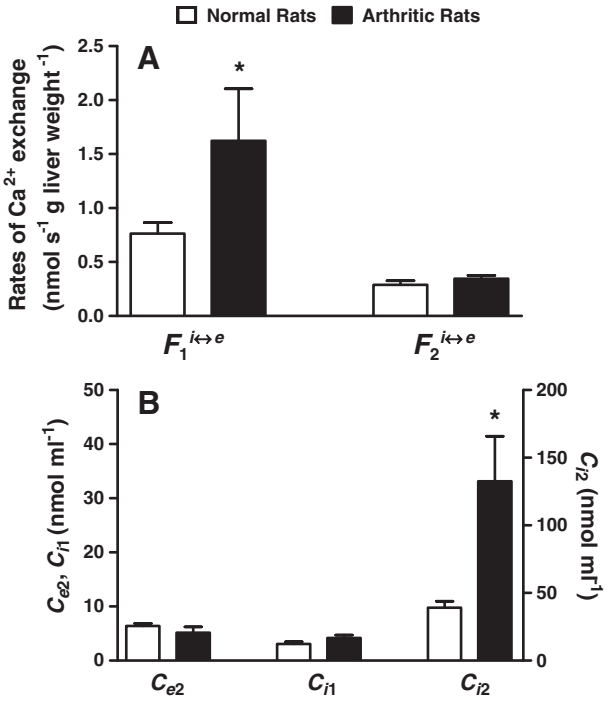

Fig. 11. Influence of the adjuvant-induced arthritis on the rates of Ca^{2+} exchange and on the Ca^{2+} pools. A: rates of Ca^{2+} exchange ($F_1^{i\leftrightarrow e}$ and $F_2^{i\leftrightarrow e}$) calculated from the transfer coefficients using Eqs. (6) and (8). B: Ca^{2+} concentrations in the extracellular rapid exchanging pool (C_{e2}) and in the cellular pools (C_{i1}, C_{i2}) calculated from the transfer coefficients using Eqs. (5), (7) and (9). Parameters for the calculations were obtained from multiple indicator-dilution experiments of the kind shown in Fig. 2A (control, white bars) and Fig. 10 (arthritic, black bars). The data are the means ± SE of 6 (normal rats) and 4 (arthritic rats) independent experiments. Significance of the differences between the means was derived from Student's *t*-test ($P \leq 0.05$). Values of arthritic rats differing statistically from those of the normal rats are labeled with an asterisk.

It should be emphasized that data obtained by the MID technique only inform about phenomena that are kinetically discernible. However, proper interpretation of the data is possible if certain reasonable assumptions about the nature of the underlying physiological processes are made. Besides the current knowledge of the nature and properties of Ca^{2+} transporters, comparison with similar kinetic studies reported by other authors can strengthen the analysis [53–55]. In the following we are discussing separately the most important topics of the present study which include not only the nature of the various calcium pools but also the modifications caused by arthritis.

4.2. The extracellular rapid exchanging Ca^{2+} pool

Comparison of the outflow profiles of [^{3}H]inulin and $^{45}Ca^{2+}$ allowed to identify a rapid extracellular exchangeable pool into which Ca^{2+} undergoes flow-limited distribution (C_{e2}). This presumably comprises the plasma membrane adjacencies including the glycocalix. This second extracellular pool was relatively small (exceeding only nearly 10% of the inulin space) and may represent Ca^{2+} bound to phospholipids and glycoproteins [56]. Actually, at least two classes of binding sites with different affinity constants have been identified in isolated plasma membranes [57,58].

Nearly 70% of the plasma membrane is facing the sinusoid [31] and in accordance with the plasma membrane lipid composition determined by Pfleger et al. [59], there are nearly 230 nmol sinusoidal phospholipid per gram liver. The concentration of Ca^{2+} in the plasma membrane (C_{e2}) at C_{e1} equal to 500 μM was 50 nmol/ml extracellular aqueous space or 111 nmol g^{-1} liver, assuming a mean value of 0.45 ml extracellular space per gram liver [43]. It seems, thus, that the amount of phospholipids in the membrane is enough to accommodate

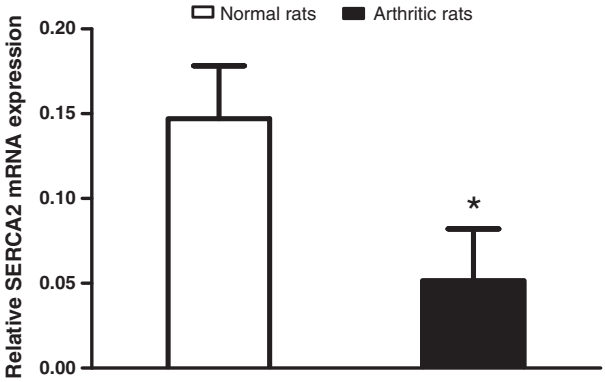

Fig. 12. Expression of SERCA2 protein in livers from normal and arthritic rats. Data are the means ± SE of independent analyses performed with livers isolated from 5 (normal) and 5 (arthritic) rats. Protein expression was normalized by 18S rRNA. (*) Significance of the differences between the means was derived from Student's *t*-test ($P \leq 0.05$).

Ca^{2+} even at concentrations higher than 500 μM. This information corroborates the kinetics of Ca^{2+} distribution indicating a single partition coefficient for the distribution of this cation between the vascular space and the plasma membrane.

4.3. The first cellular Ca^{2+} pool

That the first intracellular space represents Ca^{2+} in the cytosolic space was indicated by the large concentration gradient in relation to both the vascular space (C_{e1}) and the second extracellular space (C_{e2}). Most of this Ca^{2+} is likely to be bound to multiple cytosolic binding sites, including specific proteins such as calmodulin and regucalcin, unspecific proteins, phospholipids and metabolites [60,61]. The parabolic relation found between C_{i1} and C_{e1} may represent the binding of Ca^{2+} to sites of relatively low affinities or an increase in the affinities of the binding sites when the vascular $CaCl_2$ concentration increased (cooperative phenomenon). The possibility of a diffusion of Ca^{2+} into an additional cytosolic space, not reached at lower concentrations, can equally not be excluded. Direct measurements have indicated that at least 99% of the total cytosolic Ca^{2+} is present in bound form to several proteins and other ligand types which is in rapid equilibrium with the free form [62–65]. In consequence, the resting level of Ca^{2+} in the cytosol of unstimulated cells is around 0.1–0.2 μM at the physiological extracellular $CaCl_2$ concentration of 1.2 mM [66]. Assuming that 1% is in the free form, the free Ca^{2+} concentration in the cytosolic space at C_{e1} 500 μM from our present data would be equal to 0.81 μM. This is within the same order of magnitude of the reported free Ca^{2+} concentrations. This value is much more realistic than that estimated from the kinetic data in the perfused rat liver by L'apointe and Olson [55]. These authors estimated considerably higher Ca^{2+} concentrations in the cytosolic compartment resulting in a value of 4.2 μM for the free form.

4.4. The second cellular Ca^{2+} pool

That $^{45}Ca^{2+}$ also distributes in a deep pool within the hepatocytes (second cellular pool) could be even visually discerned by examining the tail component in the downslope of the $^{45}Ca^{2+}$ outflow profiles. It is worth to mention that when k_3 and k_4 were put equal to zero in Eq. (1) (i.e., when the second pool was omitted) it could no longer be fitted to the experimental curve. Furthermore, the calculations revealed a considerable gradient of Ca^{2+} concentration between the cytosolic (C_{i1}) and the second cellular pool (C_{i2}) which is more prominent at lower values of the former (nearly 15 times, Table 1). Apparently, there is a limited quantity of Ca^{2+}-binding sites in the second pool, the maximal capacity being already reached at low vascular Ca^{2+} concentrations, as revealed by the saturable dependence of C_{i2} from C_{i1} (Fig. 8).

Several cellular organelles such as mitochondria, nuclear envelope, the Golgi apparatus and lysosomes are able to take up and to release Ca^{2+}. It is generally recognized, however, that the endoplasmic reticulum is the largest and more controllable intracellular Ca^{2+} store in non-excitable cells [67]. In the endoplasmic reticulum Ca^{2+} may be bound to various storage proteins such as calsequestrin, calreticulins, and endoplasmins [4]. It seems thus logical to assume, in principle at least, that the second Ca^{2+} pool detected in our MID experiments comprises mainly Ca^{2+} in the endoplasmic reticulum. Even so it is worth to examine if mitochondria, which accumulate Ca^{2+} mainly in the form of calcium phosphate [68], could be equally contributing to the second cellular pool. The participation of mitochondria as a Ca^{2+} store was suggested by fractionation of hepatocytes labeled with $^{45}Ca^{2+}$ and the utilization of mitochondrial inhibitors [53]. However, the procedure for mitochondria isolation probably causes redistribution of $^{45}Ca^{2+}$ between the subcellular fractions. Mitochondrial inhibitors, on the other hand, affect Ca^{2+} distribution between the compartments since many Ca^{2+} transporters are ATP-dependent. Moreover, it is known that the Ca^{2+}-selective uniporter channel for mitochondrial Ca^{2+} uptake has a relatively low affinity for Ca^{2+}. Uptake seems to be significant only at concentrations well above the cytosolic Ca^{2+} levels [38,69]. Consistent with these findings is our observation that saturation of $^{45}Ca^{2+}$ entry into the second pool (k_3 values) occurs at low cytosolic Ca^{2+} concentrations. It is thus unlikely that under our experimental conditions the tracer had significant access to mitochondria during a single passage. It looks much likely, thus, that the second pool represents mainly the endoplasmic reticulum. We have found a maximal value of 84.1 μM for total Ca^{2+} in this space when expressed in terms of the total aqueous cell space. Assuming that the endoplasmic reticulum represents nearly 15% of the cell volume [70], the Ca^{2+} concentration in this compartment would be 6.7 fold higher (nearly 0.56 mM) if the tracer distributes uniformly. Values of 0.8 and 3.3 mM have been reported by measuring the depletion of Ca^{2+} from the endoplasmic reticulum by an ionophore or by BHQ (2,5-di-*tert*-butylhydroquinone), respectively [71].

4.5. The kinetics of Ca^{2+} exchange

The concentration gradients between the various pools discussed above ultimately reflect the corresponding ratios of the transfer coefficients for influx and efflux (i.e., k_1/k_2 and k_3/k_4). The meaning of the transfer coefficients estimated by means of the present methodology is complex. They are composite parameters, functions of the Ca^{2+} concentration in the pertinent compartment, the binding degree of Ca^{2+} to various sites, and the kinetic constants of the carrier system or systems, responsible for the transfer across membranes (basically K_M and V_{max}).

The exchange rates of Ca^{2+} between the vascular and cytosolic space ($F_1^{i \leftrightarrows e}$) and the exchange rates between the cytosolic space and the second cellular pool ($F_2^{i \leftrightarrows e}$) were saturable functions of the Ca^{2+} concentration in the pertinent space (Fig. 9). In this respect it should be mentioned that, in contrast to our results, saturation of Ca^{2+} influx was not observed in isolated hepatocytes at concentrations up to 11 mM [53,66]. Saturation was also not found in the kinetic study of L'apointe and Olson [55] in the perfused rat liver. Our results are thus consistent with the participation of transport systems even though several systems may be operating simultaneously not only in different compartments but also in different directions. These are probably the plasma membrane Ca^{2+}-ATPase (PMCA), which pumps cytosolic Ca^{2+} into the vascular space [72] and the transporters responsible for Ca^{2+} uptake into the organelles, which have been proposed to play the major roles in the maintenance of low cytosolic Ca^{2+} levels [53,66,73,5].

4.6. The action of norepinephrine

The experiments with norepinephrine were done because the actions of this hormone on Ca^{2+} fluxes and compartmentation are largely known and the results can be regarded as a test for the correctness and reliability of the methodology. The modifications in the transfer coefficients k_2, k_3 and k_4 found at 1.5 min after starting norepinephrine infusion are consistent with the known action of norepinephrine which produces a substantial increase in the cytosolic Ca^{2+} concentration. The consequence of the simultaneous diminution of k_3 and increase of k_4 is evidently an increased net efflux of Ca^{2+} from the second cellular pool which leads to increased cytosolic concentration. The diminution in k_2, on the other hand, minimizes the Ca^{2+} loss that occurs immediately after starting the infusion of norepinephrine [1,74] in consequence of the increased cytosolic concentration. No significant change in k_1 was found indicating that there was no stimulation of the inward transport systems during the first 1.5 min following norepinephrine infusion. All these observations are in agreement with the proposition that the earliest action of the Ca^{2+}-dependent hormones is the mobilization of intracellular stores and that Ca^{2+} entry into the hepatocytes occurs later on in response to the emptying of the endoplasmic reticulum-Ca^{2+} stores [1,75,5]. It should be stressed that these findings also corroborate our previous assumption that the second

intracellular pool corresponds mainly to the endoplasmic reticulum and not to the mitochondria. It should be mentioned that L'apointe and Olson [55] estimated from their kinetic analysis a reduction in the rate coefficients for Ca^{2+} efflux from the compartment corresponding to the second cellular pool under the influence of phenylephrine or vasopressin, at 50 or 500 μM extracellular $CaCl_2$. Contrary to our conclusions this observation led the authors to question if the second cellular pool corresponded to the hormone sensitive pool.

Norepinephrine increased the perfusion pressure as expected, but it also increased the vascular space. This combination of events may result from a vasoconstriction at the exit of the sinusoids because the latter phenomenon can produce distention (swelling) of the sinusoids and cells in consequence of the constant flow system employed in the present experiments [76,77].

4.7. Effects of adjuvant-induced arthritis on Ca^{2+} transport and distribution

Our experiments detected modifications on transport and distribution of Ca^{2+} in the liver of arthritic rats. The most prominent modification was the increased Ca^{2+} concentration in the hormone-sensitive cellular pool (endoplasmic reticulum). Furthermore, reduced rates of Ca^{2+} exchange between the hormone-sensitive cellular pool and the cytosolic space were also detected. The latter was consequence of diminutions in both k_4 and k_3, that of the former being more accentuated. It should be stressed that the Ca^{2+} concentration in the second cellular pool is primarily expressed in terms of the whole cell volume. Consequently, its increase also represents a real increase in Ca^{2+} content. This is true irrespective of the fact that arthritis could have produced changes in the effective volume of the endoplasmic reticulum. With respect to this possibility it should be mentioned that endoplasmic reticulum-stress, infection and inflammation can result in remodeling of the endoplasmic reticulum with changes in Ca^{2+} signaling [78,67].

The sarco-endoplasmic reticulum Ca^{2+}-ATPase (SERCA) is considered the most important system that actively pumps Ca^{2+} into the endoplasmic reticulum. The expression of SERCA2 was found to be significantly reduced in the liver of arthritic rats, a phenomenon that accounts at least partly for the diminished values of k_3. Moreover, the activity of SERCA2 has been demonstrated to depend on the phospholipid composition and on the structural state of the membrane [79,8,33]. Changes in the membrane lipid composition and in the fluidity of the endoplasmic reticulum had been earlier demonstrated in arthritis [80,81]. A reduced expression and/or activity of SERCA2 protein has been also observed in other pathological conditions including obesity [82,83] and age-related cardiac dysfunction [8,33,84].

SERCA2 plays a critical role not only in clearing cytosolic Ca^{2+} after agonist stimulations [85–87] but it is also involved in the maintenance of the resting intra-ER free calcium that controls a variety of ER-dependent cellular functions, including synthesis, folding and export of proteins, cell differentiation and ER stress response [88–90]. There is also evidence about cross-talk between the inflammatory response in the arthritis disease and the ER stress response [91–93]. Interleukin-1 (IL-1) and tumor necrosis factor-alpha (TNF-α) have been reported to induce ER stress in hepatocytes, by activating the expression and the cleavage of an ER-localized transcription factor CREBH which mediates acute phase response in the liver [92]. These proinflammatory cytokines also act as ER stressors in RA joints by up-regulating the ER chaperone (immunoglobulin-heavy-chain-binding protein) GRP78 expression in RA synoviocytes [93]. Possibly, the abnormal expression of SERCA2 is another consequence of ER stress in arthritis inflammation.

We have no definitive explanation for the k_4 reduction in livers from arthritic rats. Actually, the processes influencing the transfer coefficient k_4 under basal conditions are not well understood, since the physical structure of the elements responsible for the passive Ca^{2+} efflux or basal leaking has not yet been elucidated [94,95]. On the other hand, it is well known that, in the liver cells, inositol 1,4,5-trisphosphate receptors (IP3Rs) expressed on the ER membranes provide the main pathway for Ca^{2+} release in response to hormones like norepinephrine which act on the G-protein coupled receptors in the plasma membrane [96,97]. These receptors are modulated by many ER luminal Ca^{2+}-binding proteins such as lectin, chaperones, calreticulin and calnexin. In absolute terms the increment caused by norepineprine in k_4 was less pronounced in the arthritic livers, a finding that could be related to alterations of the expression or of the activities of IP3Rs and its modulators. It is worth noting, however, that in proportional terms norepinephrine increased k_4 by exactly the same factor (2.8) in both the normal and arthritic condition. The simplest explanation for this observation is that the efflux transport system is less active in the arthritic condition but that the sensitivity to norepinephrine is not impaired.

The change in k_4 caused by arthritis could be equally reflecting alterations in the content of Ca^{2+} binding proteins which could, in turn, be affecting the free concentration of the cation. This possibility is supported by reports about changes in the levels of the endoplasmic reticulum proteins under pathological conditions. The list includes sorcin, triadin, phosopholamban, calmyrin, calsenilin and proteins of the Bcl-2 family [98,99,67].

It should be noted that in the normal condition, the increase in k_4 caused by norepinephrine was associated with a reduction in k_3. These simultaneous changes in the transfer coefficients of influx and efflux could be related to the role of SERCA2 in controlling the frequency the of IP_3-induced intracellular Ca^{2+} oscillations [85–87]. In the arthritic condition, however, k_3 was not reduced, suggesting an alteration in this control mechanism of the Ca^{2+} fluxes that may be consequence of an altered activity/expression of SERCA2.

The observation that arthritis affects mainly the Ca^{2+} homeostasis in the endoplasmic reticulum is in accordance with recent evidence that the organelle is implicated in the pathogenesis of other diseases, including obesity [8], cardiac disorders [84], diabetes [6], Huntington's [28] and Alzheimer's diseases [29]. Independently of the mechanisms involved, it is important to stress that the lower absolute values of k_3 and k_4 under basal conditions and the differential response to norepinephrine infusion may lead to lower efficiency in mobilizing Ca^{2+} from the intracellular stores and also to replenish the stores in the arthritic condition.

5. Conclusion

It can be concluded from the bulk of the data presented in this article that the multiple-indicator dilution technique represents a useful alternative for analyzing modifications in Ca^{2+} homeostasis caused by effectors or diseases. In experimental terms the measurement of $^{45}Ca^{2+}$ outflow profiles is relatively simple and the mathematical analysis presents no significant difficulties with the now available computing facilities. The possibility of evaluating kinetics and estimating pool sizes under conditions in which hemodynamics, anatomy and hepatocyte polarity are preserved is especially attractive. In the study of the pathogenesis of liver diseases, information obtained in different cellular preparations and methodologies can be corroborated or refuted for their significance in the intact cells and whole organ. As demonstrated in the present work, the arthritis disease changes Ca^{2+} homeostasis in the intact liver by altering the endoplasmic reticulum Ca^{2+} fluxes. The observed changes in the kinetic parameters and the reduction of the SERCA2 expression were probably related to the induction of ER stress by inflammatory mediators.

Acknowledgments

This work was supported by grants from the Conselho Nacional de Desenvolvimento Científico e Tecnológico (CNPq), Coordenação de Aperfeiçoamento de Pessoal do Ensino Superior (CAPES) and Programa de Núcleos de Excelência (PRONEX) do CNPq e Fundação Araucária do Estado do Paraná. Karina Sayuri Utsunomiya holds fellowships from the Conselho Nacional de Desenvolvimento Científico e Tecnológico

(CNPq) and Coordenação de Aperfeiçoamento de Pessoal de Nível Superior (CAPES). The authors especially thank Dr. Coen C. Paulusma for his assistance on measurements of SERCA2 expression.

References

[1] P.H. Reinhart, W.M. Taylor, F.L. Bygrave, The action of α-adrenergic agonists on plasma-membrane calcium fluxes in perfused rat liver, Biochem. J. 220 (1984) 43–50.
[2] M.J. Berridge, The endoplasmic reticulum: a multifunctional signaling organelle, Cell Calcium 32 (2002) 235–249.
[3] L.D. Gaspers, A.P. Thomas, Calcium signaling in liver, Cell Calcium 38 (2005) 329–342.
[4] N.-E.L. Saris, E. Carafoli, A historical review of cellular calcium handling, with emphasis on mitochondria, Biochemistry 70 (2005) 187–194.
[5] G.J. Barritt, J. Chen, G.Y. Rychkov, Ca^{2+}-permeable channels in the hepatocyte plasma membrane and their roles in hepatocyte physiology, Biochim. Biophys. Acta 1783 (2008) 651–672.
[6] D.L. Eizirik, A.K. Cardozo, M. Cnop, The role for endoplasmic reticulum stress in diabetes mellitus, Endocr. Rev. 29 (2008) 42–61.
[7] J.W. Ramadan, S.R. Steiner, C.M. O'Neill, C.S. Nunemaker, The central role of calcium in the effects of cytokines on beta-cell function: implications for type 1 and type 2 diabetes, Cell Calcium 50 (2011) 481–490.
[8] S. Fu, L. Yang, P. Li, O. Hofmann, L. Dicker, W. Hide, X. Lin, S.M. Watkins, A.R. Ivanov, G.S. Hotamisligil, Aberrant lipid metabolism disrupts calcium homeostasis causing liver endoplasmic reticulum stress in obesity, Nature 473 (2011) 528–530.
[9] B.D. Lowes, E.M. Gilbert, W.T. Abraham, W.A. Minobe, P. Larrabee, D. Ferguson, E.E. Wolfel, J. Linderfeld, T. Tsvetkova, A.D. Robertson, R.A. Quaife, M.R. Bristow, Myocardial gene expression in dilated cardiomyopathy treated with beta-blocking agents, N. Engl. J. Med. 346 (2002) 1357–1365.
[10] C.W. Distelhorst, M.D. Bootman, Bcl-2 interaction with the inositol 1,4,5-trisphosphate receptor: role in Ca^{2+} signaling and disease, Cell Calcium 50 (2011) 234–241.
[11] A. Varadi, G.A. Rutter, Dynamic imaging of endoplasmic reticulum Ca^{2+} concentration in insulin-secreting MIN6 cells using recombinant targeted cameleons: roles of sarco(endo)plasmic reticulum Ca^{2+}-ATPase (SERCA)-2 and ryanodine receptors, Diabetes 51 (2002) S190–S201.
[12] D.R. Laybutt, A.M. Preston, M.C. Akerfeldt, J.G. Kench, A.K. Busch, A.V. Biankin, T.J. Biden, Endoplasmic reticulum stress contributes to beta cell apoptosis in type 2 diabetes, Diabetologia 50 (2007) 752–763.
[13] H. Lu, V. Koshkin, E.M. Allister, A.V. Gyulkhandanyan, M.B. Wheeler, Molecular and metabolic evidence for mitochondrial defects associated with beta-cell dysfunction in a mouse model of type 2 diabetes, Diabetes 59 (2010) 448–459.
[14] E.H.S. Choy, G.S. Panayi, Cytokine pathways and joint inflammation in rheumatoid arthritis, N. Engl. J. Med. 344 (2001) 907–916.
[15] J.L. Humes, R.J. Bonney, L. Pelus, M.E. Dahlgren, S.J. Sadowski, F.A. Kuehl Jr., P. Davies, Macrophages synthesise and release prostaglandins in response to inflammatory stimuli, Nature 269 (1977) 149–151.
[16] S.H. Ferreira, Inflammatory pain, prostaglandin hyperalgesia and the development of peripheral analgesics, Trends Pharmacol. Sci. 2 (1981) 183–186.
[17] P. Kahle, J.G. Saal, K. Schaudt, J. Zacher, P. Fritz, G. Pawelec, Determination of cytokines in synovial fluids: correlation with diagnosis and histomorphological characteristics of synovial tissue, Ann. Rheum. Dis. 51 (1992) 731–734.
[18] H. Sano, T. Hla, J.A. Maier, L.J. Crofford, J.P. Case, T. Maciag, R.L. Wilder, In vivo cyclooxygenase expression in synovial tissues of patients with rheumatoid arthritis and osteoarthritis and rats with adjuvant and streptococcal cell wall arthritis, J. Clin. Invest. 89 (1992) 97–108.
[19] T. Hamada, N. Arima, M. Shindo, K. Sugama, Y. Sasaguri, Suppression of adjuvant arthritis of rats by a novel matrix metalloproteinase-inhibitor, Br. J. Pharmacol. 131 (2000) 1513–1520.
[20] M. Stolina, G. Schett, D. Dwyer, S. Vonderfecht, S. Middleton, D. Duryea, E. Pacheco, G. Van, B. Bolon, U. Feige, D. Zack, P. Kostenuik, RANKL inhibition by osteoprotegerin prevents bone loss without affecting local or systemic inflammation parameters in two rat arthritis models: comparison with anti-TNFα or anti-IL-1 therapies, Arthritis Res. Ther. 11 (2009) R187.
[21] M.E. Billingham, Models of arthritis and the search for anti-arthritic drugs, Pharmacol. Ther. 21 (1983) 389.
[22] E. Brahn, Animal models of rheumatoid arthritis. Clues to etiology and treatment, Clin. Orthop. Relat. Res. 265 (1991) 42–53.
[23] S.M. Caparroz-Assef, C.A. Bersani-Amado, E.A. Nascimento, A.M. Kelmer-Bracht, E.L. Ishii-Iwamoto, Effects of the nonsteroidal anti-inflammatory drug nimesulide on energy metabolism in livers from adjuvant-induced arthritic rats, Res. Commun. Pathol. Pharmacol. 99 (1998) 93–116.
[24] Z. Fedatto Júnior, A.M. Kelmer-Bracht, E.L. Ishii-Iwamoto, J. Constantin, A. Bracht, Gluconeogenesis in the liver of arthritic rats, Cell Biochem. Funct. 17 (1999) 271–278.
[25] Z. Fedatto Júnior, E.L. Ishii-Iwamoto, C.A. Bersani Amado, E.R. Martins Maciel, A. Dúrso Panerari, A. Bracht, A.M. Kelmer-Bracht, Glucose phosphorylation capacity and glycolysis in the liver of arthritic rats, Inflamm. Res. 49 (2000) 128–132.
[26] Z. Fedatto Júnior, E.L. Ishii-Iwamoto, S.M. Caparroz-Assef, G. Vicentini, A. Bracht, A.M. Kelmer-Bracht, Glycogen levels and glycogen catabolism in livers from arthritic rats, Mol. Cell. Biochem. 229 (2002) 1–7.
[27] P. Yassuda Filho, A. Bracht, E.L. Ishii-Iwamoto, S.H. Lousano, L. Bracht, A.M. Kelmer-Bracht, The urea cycle in the liver of arthritic rats, Mol. Cell. Biochem. 243 (2003) 97–106.
[28] I. Bezprozvanny, M.R. Hayden, Deranged neuronal calcium signaling and Huntington disease, Biochem. Biophys. Res. Commun. 322 (2004) 1310–1317.
[29] I. Bezprozvanny, M.P. Mattson, Neuronal calcium mishandling and the pathogenesis of Alzheimer's disease, Trends Neurosci. 31 (2008) 454–463.
[30] Å. Björck, G. Dahlquist, Numerische Methoden, Oldenburg Verlag, Munich, 1972.
[31] A. Blouin, R.P. Bolender, E.R. Weibel, Distribution of organelles and membranes between hepatocytes and nonhepatocytes in the rat liver parenchyma. A stereological study, J. Cell Biol. 72 (1977) 441–455.
[32] A. Bracht, A.J. Schwab, R. Scholz, Untersuchung von Flussgeschwindigkeiten in der isolierten perfundierten Rattenleber durch Pulsmarkierung mit radioaktiven Substraten und mathematischer Analyse der Auswaschkinetiken, H.-S. Z, Phys. Chem. 361 (1980) 357–377.
[33] M.K. Strosova, J. Karlovska, P. Zizkova, M. Kwolek-Mirek, S. Ponist, C.M. Spickett, L. Horakova, Modulation of sarcoplasmic/endoplasmic reticulum Ca^{2+}-ATPase activity and oxidative modification during the development of adjuvant arthritis, Arch. Biochem. Biophys. 511 (2011) 40–47.
[34] G.J. Barritt, M.W. Whitehouse, Pathobiodynamics: effect of extrahepatic inflammation on calcium transport and drug metabolism by rat liver mitochondria in vitro, Biochem. Med. 17 (1977) 99–115.
[35] P.M. Souza Silva, E. Tanabe, A.P. Munhos Hermoso, C.A. Bersani-Amado, A. Bracht, E.L. Ishii-Iwamoto, C.L. Salgueiro-Pagadigorria, Changes in calcium-dependent membrane permeability properties in mitochondria of livers from arthritic rats, Cell Biochem. Funct. 26 (2008) 443–450.
[36] J.N. Crofts, G.J. Barritt, The measurement of Ca^{2+} inflow across the liver cell plasma membrane by using Quin2 and studies of the roles of Na^{+} and extracellular Ca^{2+} in the mechanism of Ca^{2+}-inflow, Biochem. J. 264 (1989) 61–70.
[37] G. Rychkov, H.M. Brereton, M.L. Harland, G.J. Barritt, Plasma membrane Ca^{2+} release-activated Ca^{2+} channels with a high selectivity for Ca^{2+} identified by patch-clamp recording in rat liver cells, Hepatology 33 (2001) 938–947.
[38] B. Moreau, C. Nelson, A.B. Parekh, Biphasic regulation of mitochondrial Ca^{2+} uptake by cytosolic Ca^{2+} concentration, Curr. Biol. 16 (2006) 1672–1677.
[39] M.M. Zegers, D. Hoekstra, Mechanisms and functional features of polarized membrane traffic in epithelial and hepatic cells, Biochem. J. 336 (1998) 257–269.
[40] C.A. Goresky, G.G. Bach, B.E. Nadeau, On the uptake of materials by the intact liver: the transport and net removal of galactose, J. Clin. Invest. 52 (1973) 991–1009.
[41] C.A. Goresky, D.S. Daly, S. Mishkin, I.M. Arias, Uptake of labeled palmitate by the intact liver: role of intracellular binding sites, Am. J. Physiol. 234 (1978) E542–E553.
[42] A.J. Schwab, A. Bracht, R. Scholz, Transport of D-lactate in perfused rat liver, Eur. J. Biochem. 102 (1979) 537–547.
[43] O. Ferraresi-Filho, E.L. Ishii-Iwamoto, A. Bracht, Transport, metabolism and distribution space of octanoate in the perfused rat liver, Cell Biochem. Funct. 15 (1997) 69–80.
[44] C.M. Pearson, F.D. Wood, Studies of arthritis and other lesions induced in rats by the injection of mycobacterial adjuvant, Am. J. Pathol. 42 (1963) 93–95.
[45] S.M. Caparroz-Assef, C.A. Bersani-Amado, A.M. Kelmer-Bracht, A. Bracht, E.L. Ishii-Iwamoto, The metabolic changes caused by dexamethasone in the adjuvant-induced arthritic rat, Mol. Cell. Biochem. 302 (2007) 87–98.
[46] A. Bracht, E.L. Ishii-Iwamoto, A.M. Kelmer-Bracht, O estudo do metabolismo no fígado em perfusão, in: A. Bracht, E.L. Ishii-Iwamoto (Eds.), Métodos de Laboratório em Bioquímica, Manole, São Paulo, 2003, pp. 274–288.
[47] C.A. Goresky, W.H. Ziegler, G.G. Bach, Capillary exchange modeling: barrier-limited and flow-limited distribution, Circ. Res. 27 (1970) 739–764.
[48] C.P. Rose, C.A. Goresky, G.G. Bach, The capillary and sarcolemmal barriers in the heart. An exploration of labeled water permeability, Circ. Res. 41 (1977) 515–533.
[49] O. Ferraresi-Filho, Transporte e metabolismo de octanoato no fígado de rato (Doctoral thesis), 1993, pp. 217.
[50] C.A. Goresky, A linear method for determining liver sinusoidal and extravascular volumes, Am. J. Physiol. 204 (1963) 626–640.
[51] P. Meier, K.L. Zierler, On the theory of the indicator dilution method for measurement of blood flow and volume, J. Appl. Physiol. 6 (1954) 731–744.
[52] S. Wagon, Mathematica in Action, Second ed. Springer-Verlag, New York, 1999.
[53] J.C. Parker, G.J. Barritt, J.C. Wadsworth, A kinetic investigation of the effects of adrenaline on $^{45}Ca^{2+}$ exchange in isolated hepatocytes at different Ca^{2+} concentrations, at 20 °C and in the presence of inhibitors of mitochondrial Ca^{2+} transport, Biochem. J. 216 (1983) 51–62.
[54] R.G. Gish, C. Garcia, T. Reed, N. Kaplowitz, G.A. Langer, Calcium compartmentation and exchange rates in primary hepatocyte culture, Anal. Biochem. 187 (1990) 187–196.
[55] D.S. L'apointe, M.S. Olson, Compartmental analysis of $^{45}Ca^{2+}$ efflux in perfused rat liver: effects of hormonal stimulation, Cell Calcium 12 (1991) 743–753.
[56] J.A. Post, G.A. Langer, J.A.F. op den Kamp, A.J. Verkleij, Phospholipid asymmetry in cardiac sarcolemma. Analysis of intact cell and "gas-dissected" membranes, Biochim. Biophys. Acta 943 (1988) 256–266.
[57] L. Shlatz, G.V. Marinetti, Calcium binding to the rat liver plasma membrane, Biochim. Biophys. Acta 290 (1972) 70–83.
[58] A.M. Chambault, F. Leray-Pecker, G. Feldman, J. Hanoune, Calcium binding properties and ATPase activities of rat liver plasma membranes, J. Gen. Physiol. 64 (1974) 104–126.
[59] R.C. Pfleger, N.G. Anderson, F. Snyder, Lipid class and fatty acid composition of rat liver plasma membranes isolated by zonal centrifugation, Biochemistry 7 (1986) 2826–2833.
[60] R.J.P. Williams, Biochemistry of sodium, potassium, magnesium and calcium, Q. Rev. Chem. Soc. 24 (1970) 331–361.
[61] E. Carafoli, Intracellular calcium homeostasis, Ann. Rev. Biochem. 56 (1987) 395–433.
[62] M. Yoshida, Y. Tada, Y. Kasahara, K. Ando, E. Satoyoshi, Ca content of human erythrocytes—what is the true value? Cell Calcium 7 (1986) 169–174.

[63] J. Meldolesi, L. Madeddu, T. Pozzan, Intracellular Ca^{2+}-storage organelles in nonmuscle cells: heterogeneity and functional assignment, Biochim. Biophys. Acta 1055 (1990) 130–140.
[64] E. Neher, G.J. Augustine, Calcium gradients and buffers in bovine chromaffin cells, J. Physiol. 450 (1992) 273–301.
[65] J.R. Berlin, J.W.M. Bassani, D.M. Bers, Intrinsic cytosolic calcium buffering properties of single rat cardiac muscle, Biophys. J. 67 (1994) 1775–1787.
[66] B.P. Hughes, A.M. Auld, G.J. Barritt, Effect of extracellular Ca^{2+} on plasma membrane Ca^{2+} inflow and cytoplasmic free Ca^{2+} in isolated hepatocytes, Biochim. Biophys. Acta 928 (1987) 208–216.
[67] E. Sammels, J.B. Parys, L. Missiaen, H. de Smedt, G. Bultynck, Intracellular Ca^{2+} storage in health and disease: a dynamic equilibrium, Cell Calcium 47 (2010) 297–314.
[68] K.E. Coll, S.K. Joseph, B.E. Corkey, J.R. Williamson, Determination of matrix free Ca^{2+} concentration and kinetics of Ca^{2+} efflux in liver and heart mitochondria, J. Biol. Chem. 257 (1982) 8696–8704.
[69] S. de la Fuente, P. Montenegro, R.I. Fonteriz, A. Moreno, C.D. Lobatón, M. Montero, J. Alvarez, The dynamics of mitochondrial Ca^{2+} fluxes, Biochim. Biophys. Acta 1797 (2010) 1727–1735.
[70] E.R. Weibel, W. Staubli, H.R. Gnagi, F.A. Hess, Correlated morphometric and biochemical studies on the liver cell, J. Cell Biol. 42 (1969) 68–91.
[71] F.L. Bygrave, A. Benedetti, What is the concentration of calcium ions in the endoplasmic reticulum? Cell Calcium 19 (1996) 547–551.
[72] E. Carafoli, Biogenesis: plasma membrane calcium ATPase: 15 years of work on the purified enzyme, FASEB J. 8 (1994) 993–1002.
[73] J.N. Crofts, G.J. Barritt, The liver-cell plasma-membrane Ca^{2+}-inflow systems exhibit a broad specificity for divalent metal ions, Biochem. J. 269 (1990) 579–587.
[74] N.S. Yamamoto, E.L. Ishii-Iwamoto, A. Bracht, Activation of glycogenolysis by methotrexate, Biochem. Pharmacol. 44 (1992) 781–787.
[75] J.W. Putney Jr., D.L. Aub, C.W. Taylor, J.E. Merritt, Formation and biological action of inositol 1,4,5-trisphosphate, Fed. Proc. 45 (1986) 2634–2638.
[76] V.C. Minguetti-Câmara, J. Constantin, F. Suzuki-Kemmelmeier, E.L. Ishii-Iwamoto, A. Bracht, Hepatic heterogeneity in the response to ATP studied in the bivascularly perfused rat liver, Mol. Cell. Biochem. 179 (1998) 35–48.
[77] A. Polato-Schmeisch, F. Suzuki-Kemmelmeier, A. Bracht, The Ca^{2+} mediated metabolic hemodynamic effects of vasopressin in the liver, Trends Cell Mol. Biol. 1 (2005) 35–50.
[78] M. Lebiedzinska, G. Szabadkai, A.W.E. Jones, J. Duszynski, M.R. Wieckowski, Interactions between the endoplasmic reticulum, mitochondria, plasma membrane and other subcellular organelles, Int. J. Biochem. Cell Biol. 41 (2009) 1805–1816.
[79] S.M. Lee, J.W. Lee, Y.S. Song, D.Y. Hwang, Y.K. Kim, S.Y. Nam, D.J. Kim, Y.W. Yun, D.Y. Yoon, J.T. Hong, Ryanodine receptor-mediated interference of neuronal cell differentiation by presenilin 2 mutation, J. Neurosci. Res. 82 (2005) 542–550.
[80] S. Ishizuki, E. Fujihira, Peroxidative status of isolated hepatocytes from adjuvant arthritic rats, Res. Commun. Chem. Pathol. Pharmacol. 44 (1984) 431–443.
[81] G. Nemez, P. Bor, I. Lepran, M. Koltai, L. Szekeres, Membrane phospholipids and fatty acid changes in the mitochondrial and sarcolemmal fractions in adjuvant arthritic rats, J. Mol. Cell. Cardiol. 18 (1986) 739–747.
[82] S.W. Park, Y.J. Zhou, J. Lee, J. Lee, U. Ozcan, Sarco(endo) plasmic reticulum Ca^{2+}-ATPase 2b is a major regulator of endoplasmic reticulum stress and glucose homeostasis in obesity, Proc. Natl. Acad. Sci. U.S.A. 107 (2010) 19320–19325.
[83] S. Fu, L. Yang, P. Li, O. Hofmann, L. Dicker, W. Hide, X. Lin, S.M. Watkins, A.R. Ivanov, G.S. Hotamisligi, Aberrant lipid metabolism disrupts calcium homeostasis causing liver endoplasmic reticulum stress in obesity, Nature 473 (2011) 528–531.
[84] Q. Jiao, H. Takeshima, Y. Ishikawa, S. Minamisawa, Sarcalumenin plays a critical role in age-related cardiac dysfunction due to decreases in SERCA2a expression and activity, Cell Calcium 51 (2012) 31–39.
[85] P. Camacho, J. Lechleiter, Increased frequency of calcium waves in *Xenopus laevis* oocytes that express a calcium-ATPase, Science 260 (1994) 226–229.
[86] L.M. John, J.D. Lechleiter, P. Camacho, Differential modulation of SERCA2 isoforms by calreticulin, J. Cell Biol. 142 (1998) 963–973.
[87] K. Thurley, A. Skupin, R. Thul, M. Falcke, Fundamental properties of Ca^{2+} signals, Biochim. Biophys. Acta 1820 (2012) 1185–1194.
[88] C.M. Misquitta, D.P. Mack, A.K. Grover, Sarco/endoplasmic reticulum Ca^{2+} (SERCA)-pumps: link to heart beats and calcium waves, Cell Calcium 25 (1999) 277–290.
[89] F. Wuytack, L. Raeymaekers, L. Missiaen, Molecular physiology of the SERCA and SPCA pumps, Cell Calcium 32 (2002) 279–305.
[90] K. Zhang, X. Shen, J. Wu, K. Sakaki, T. Saunders, D.T. Rutkowski, S.H. Back, R.J. Kaufman, Endoplasmic reticulum stress activates cleavage of CREBH to induce a systemic inflammatory response, Cell 124 (2006) 587–599.
[91] X. Xue, J.H. Piao, A. Nakajima, S. Sakon-Komazawa, Y. Kojima, K. Mori, H. Yagita, K. Okumura, H. Harding, H. Nakano, Tumor necrosis factor α (TNFα) induces the unfolded protein response (UPR) in a reactive oxygen species (ROS)-dependent fashion, and the UPR counteracts ROS accumulation by TNFα, J. Biol. Chem. 280 (2005) 33917–33925.
[92] K. Zhang, X. Shen, J. Wu, K. Sakaki, T. Saunders, D.T. Rutkowski, S.H. Back, R.J. Kaufman, Endoplasmic reticulum stress activates cleavage of CREBH to induce a systemic inflammatory response, Cell 124 (2006) 587–599.
[93] K. Zhang, R.J. Kaufman, From endoplasmic-reticulum stress to the inflammatory response, Nature 24 (2008) 455–462.
[94] F. van Coppenolle, F.V. Abeele, C. Slomianny, M. Flourakis, J. Hesketh, E. Dewailly, N. Prevarskaya, Ribosome–translocon complex mediates calcium leakage from endoplasmic reticulum stores, J. Cell Sci. 117 (2004) 4135–4142.
[95] R. Giunti, A. Gamberucci, R. Fulceri, G. Bánhegyi, A. Benedetti, Both translocon and a cation channel are involved in the passive Ca^{2+} leak from the endoplasmic reticulum: a mechanistic study on rat liver microsomes, Arch. Biochem. Biophys. 462 (2007) 115–121.
[96] J.K. Foskett, C. White, K.H. Cheung, D.O.D. Mak, Inositol trisphosphate receptor Ca^{2+} release channels, Physiol. Rev. 87 (2007) 593–658.
[97] M.J. Berridge, Inositol trisphosphate and calcium signalling mechanisms, Biochim. Biophys. Acta 1793 (2009) 933–940.
[98] H. He, M. Lam, T.S. McCormick, C.W. Distelhorst, Maintenance of calcium homeostasis in the endoplasmic reticulum by Bcl-2, J. Cell Biol. 138 (1997) 1219–1228.
[99] J.J. Mackrill, Protein–protein interactions in intracellular Ca^{2+}-release channel function, Biochem. J. 337 (1999) 345–361.